Science Advances
AAAS

FRONT MATTER

Title

- Single cell assessment of human stem cell derived mesolimbic models and their responses to substances of abuse.
- Organoid exposure to substances of abuse.

Authors

Example: Thomas P. Rudibaugh[1,†], Ryan W. Tam[1,†], R. Chris Estridge[1], Albert J. Keung[1,*]

Affiliations

[1]Department of Chemical and Biomolecular Engineering, North Carolina State University, Raleigh, NC 27606.

[†]Equal Contribution

[*]Corresponding Author
Correspondence: ajkeung@ncsu.edu

Abstract

The mesolimbic pathway connects ventral tegmental area dopaminergic neurons and striatal medium spiny neurons, playing a critical role in reward and stress behaviors. Exposure to substances of abuse during development and adulthood has been linked to adverse outcomes and molecular changes. The rise of human cell repositories and whole genome sequences enables human functional genomics 'in a dish', offering insights into human-specific responses to substances of abuse. Characterizations of *in vitro* models are necessary to ensure appropriate experimental designs and accurate interpretation of results. This study provides a comprehensive characterization of these models and their responses to substances of abuse, introducing new culture conditions for generating medium spiny neurons and dopaminergic neurons from human pluripotent stem cells. Single cell analysis reveals cell type-specific transcriptomic responses to dopamine, cocaine, and morphine, including compound and cell type-specific transcriptomic signatures related to neuroinflammation and alterations in signaling pathways. These findings offer a resource for future genomics studies leveraging human stem cell-derived models.

Teaser

Generation and characterization of a novel mesolimbic pathway model and its response to acute dopamine, morphine, and cocaine.

MAIN TEXT

Introduction

The mesolimbic "reward" pathway refers to the dopaminergic innervation of ventral tegmental area (VTA) dopaminergic neurons (DN) onto the medium spiny neurons (MSN) of the striatum. Signaling in this pathway regulates reward and stress behaviors, and pathway alterations either during development or adulthood are linked to a number of neurological disorders including schizophrenia and addiction[1–3]. Substances of abuse can act on this pathway through diverse mechanisms still being discovered including opioids or ethanol binding to μ-opioid receptors, and stimulants such as cocaine and amphetamines increasing the amount and duration of presynaptic dopamine impinging onto MSNs[4–10]. It is also possible and perhaps likely that these substances have additional impacts on neuronal and non-neuronal cell physiology, especially during early neurodevelopment. Exposure to these substances have been observed to drive many epigenetic, transcriptomic, structural, and synaptic changes both in adult MSNs and *in utero*[11–15].

Our current understanding of cells of the mesolimbic pathway and their interactions with substances of abuse derives largely from rodent models and human epidemiological studies[16–19]. The rapid growth of human cell repositories, reprogramming technologies, and omics methods are driving considerable excitement for the potential of also performing human functional genomics in a dish. As an example, banked blood samples from hundreds to thousands of human donors can now be induced into pluripotent stem cells (hPSC) and then subsequently differentiated into target cell and organoid models. These models provide researchers the intriguing possibilities of performing experimental perturbations, identifying the effects of disease-linked mutations, and also capturing the magnitude and scale of effects driven by diverse human genetic backgrounds[20–35]. There is also increasing interest and needs for such models in preclinical testing[36]. However, these experimental models are still in their infancy with their utility limited by incomplete molecular and cellular characterization and variability in basal media compositions.

As a few example challenges related to mesolimbic cell types: multiple distinct models have been developed without clear comparisons of how they differ in cellular composition and responsiveness[23–26,30–32,37–46]; most ventral forebrain organoids have not been characterized for their ability to generate MSNs[32,45]; it is unknown what the differences are between 2D and 3D models; it is a widely held, but not validated, assumption that 2D models are almost homogeneous systems especially compared to 3D organoids; it is unclear which cell types are driving responses measured in bulk to perturbations such as substances of abuse or microenvironmental factors; and finally, though not exclusively, as more complex systems are built from hPSC-derived cells, such as assembloids to model connections between brain regions, cell culture and media conditions will need to be engineered to be simultaneously compatible with the multiple neuronal or organoid systems being combined together. Therefore, it will be important to rigorously characterize, compare, and establish baseline datasets for these systems; these datasets will support the efficient and rigorous investment, design, and interpretation of expensive functional genomics experiments as well as of association studies.

Through single cell RNA sequencing (scRNAseq) and immunohistochemistry we quantitatively compare seven 2D and 3D models for their abilities to generate MSNs[32,34,45 23,26,30,32,44,45]. We also develop two novel models with the purpose of creating media conditions compatible with cocultures or assembloids. We then expose hPSC-derived organoids and assembloids to physiologically relevant doses of dopamine, cocaine, and morphine, perform scRNAseq, and identify cell-type specific transcriptional responses. This work provides new experimental frameworks and benchmarks for the use of hPSCs to model MSNs and DNs, provides direct comparisons between 2D and 3D systems, and reveals

transcriptomic programs activated in these models in response to substances of abuse that may be relevant to long-term neuroplastic alterations observed in the mesolimbic pathway. These data and analyses serve as a resource for the design of future *in vitro* studies related to substance use disorders and *in utero* drug exposures, as well as to human stem cell derived models more generally.

Results

Development of striatal and midbrain organoids compatible with early assembloid generation

Our overall goals are to establish baseline comparisons of 2D and 3D models containing MSNs and DNs (with a focus on MSNs) by mapping their cellular compositions via scRNAseq, and to assess transcriptomic responses of a subset of these models to substances of abuses. However, we first take the opportunity to develop two new models that may fill existing gaps in contemporary experimental capabilities, with the goal that they can be included in our comparison of models.

Two key cell types of the mesolimbic pathway are MSNs expressing DARPP32 and DNs expressing tyrosine hydroxylase (TH). Both 2D neuronal and 3D cerebral organoid protocols have been regionally specified toward forebrain and midbrain lineages that are expected to include MSNs and DNs, respectively. However, while several 2D protocols have been shown to generate MSNs[23,26,30,43,44] and DNs[31,39,40,46–51], and 3D midbrain organoid protocols have been shown to generate DNs[24,25,27], it is unclear if 3D forebrain organoids contain MSNs[32,45]. In addition, given the longer developmental timescales of organoid models, it would be useful in the future to be able to physically merge DN- and MSN-containing organoids into assembloids to simulate more complex neural pathways and projections. This is not currently possible as current forebrain and midbrain models are differentiated and cultured in different basal medias. With these two considerations in mind, our first goals are to develop one new organoid model, each, with forebrain and midbrain regional specifications that use media conditions mutually compatible with early fusion (at day 25). We also assess the expression of DARPP32 and other MSN markers in previously developed forebrain organoid models through immunostaining and RT-qPCR, prior to a comprehensive scRNAseq comparison of both the new and existing models.

Existing organoid models use a progression of basal media with varying compositions that are distinct from one another, for example in the balances of DMEM:F12 and neurobasal media, N2 supplement, and knockout serum replacement, among many other components. In addition, the lengths of patterning steps are highly variable between models and often extend well over four weeks. We also note that prior work generating forebrain organoids[32,45] focused on the use of sonic hedgehog (SHH) to drive cells towards ventral fates deriving from the medial ganglionic eminence (MGE), yet striatal MSNs derive from the less ventral lateral ganglionic eminence (LGE) (Figure 1A-B). To address both of these issues, we begin with the whole brain organoid model developed by Lancaster and colleagues[34] to provide a common basal media, as this media is the most 'permissive' of different regional specifications. We then layer on patterning factors informed by 2D differentiation models.

Specifically, to target enrichment of forebrain striatal neurons, we begin with the basal media of the whole brain organoid model and add a combination of WNT inhibition by DKK-1 for anterior patterning, and moderate BMP activation by Activin A for medial dorso-ventral striatal development (Figure 1A-B, "Rudibaugh1"). This strategy draws upon prior derivations of 2D striatal neurons[30,52]. Five days after patterning is complete (day 30, D30), these organoids contain cells positive for the early striatal marker GSX2 and by D90 contain DARRP32+/CTIP2+ striatal neurons (Figures S1A-B). Among the three methods, the Bagley protocol produces the highest percentage of DARPP32+/MAP2+ neurons (Figure 1C). In addition, the Bagley organoids were found to be GSX2+ at D30 and DARPP32+/CTIP2+ at D90 (Figure S1C-D). The Rudibaugh1, Bagley, and Xiang-Tanaka models also express striatal markers

DARPP32, *A2A*, *TAC1*, and *PENK*, at levels enriched over undifferentiated hPSCs as measured by RT-qPCR at D90 (Figures 1F, S1G-I).

To create midbrain organoids containing DNs, we again begin with the basal media of the whole brain organoid model and add a combination of SHH, WNT, and FGF pathway activators in line with previous 2D patterning methods[31] (Figure 1A-B, "Rudibaugh2"). At D30, these organoids contain cells expressing the developing midbrain marker FOXA2[30,31] and contain TH+/NURR1+ DNs (Figures 1D, S1E-I). These organoids also express DN markers *DAT*, *NURR1*, *DDC*, and *TH* at levels greater than Bagley and Rudibaugh1 organoids and undifferentiated hPSCs (D90, Figures 1G, S1H-I).

Reassuringly, the forebrain and midbrain organoids are all enriched for MSN and DN marker expression, respectively, relative to each other as well as to undifferentiated hPSCs (Figures 1F-G). Importantly, the patterning for both Rudibaugh1 and Rudibaugh2 models are complete by D25 at which point both organoid models could continue to mature in identical media and be fused to form an assembloid. We also note that the forebrain organoid model developed by Bagley and colleagues[32] is also derived from the whole brain protocol[34], and could be used in conjunction with the Rudibaugh2 model to create assembloids.

scRNAseq reveals heterogeneous compositions and distinct enrichments of GABAergic subtypes in seven 3D and 2D striatal models

Immunostaining and RT-qPCR indicate two previously developed forebrain organoid models (Xiang-Tanaka and Bagley)[32,45] do express striatal markers. Furthermore, the new forebrain (Rudibaugh1) and midbrain (Rudibaugh2) models, designed to share basal media components, contain striatal and dopaminergic cells, respectively. With confirmation that striatal neurons exist in the three 3D forebrain models (Xiang-Tanaka, Bagley, and Rudibaugh1)[32,45], we next perform scRNAseq alongside four D45 hPSC-derived 2D striatal neuron models (Arber, Wu, Nicoleau, and Fjodorova)[23,26,30,44], and ask how each model, and whether dimensionality, generally affects cell type composition (Figure 2A)[23,26,30,32,44,45]. We chose D90 3D organoids and D45 2D neural cultures as most publications cite these time points for stably matured and differentiated neuronal models.

Using combinations of marker genes as previously described[53], we identify 34 distinct cell clusters comprising 8 broader cell classifications (Figures 2B-C, S2A). The broader cell classifications include *GAD1+* GABAergic neurons, *SLC17A6+* glutamatergic neurons, *CNTNAP2+ or RBFOX1+* interneurons, *TOP2A+* progenitors, *GLI3+* radial glia, *GFAP+* astrocytes, *TMEM132D+* oligodendrocytes, and *USPL1+* mesenchymal stem cells. The specific genes associated with each classification are not the only ones defining each cell classification but are useful in presentation and discussion. As expected for organoid systems, the three striatal organoids show significant heterogeneity, with less than 40% of the cells being GABAergic neurons (Figure 2D). However, what is surprising is the status of the 2D models. 2D models are often presumed to be relatively homogeneous at this time point, or at least more so than what organoids achieve at any time point; yet they show a similar level of heterogeneity to the 3D models, with substantial percentages of GABAergic neurons, glutamatergic neurons, interneurons, oligodendrocytes, astrocytes, and stem and progenitor cells. In addition, there are no media components in the remaining maturation media that would be expected to direct remaining stem cells and progenitors to differentiate, or non-neuronal cells to be selected away, if the culture time were extended further.

We next narrow our analysis to ask if these models are enriched for specific subtypes of GABAergic neurons, seeking to identify a subcluster(s) that mimics MSNs of the striatum. There are five different subclusters of GABAergic neurons identified and each model generates a different proportion of each subcluster (Figure S2B). We observe enrichment of the GABAergic neuron 1 subcluster in the Rudibaugh1, Fjodorova, Wu, and Nicoleau models (Figures 2E-F, S2B). This subcluster expresses lower

levels of GABAergic *GAD1* and *GAD2* and higher levels of glutamatergic *GRIN2A* and *GRM5* when compared to the other GABAergic neuron subclusters (Figure S2C). This suggests these are relatively immature neurons that express both GABAergic and Glutamatergic neuron markers, observed early in neurodevelopment as both neurotransmitters play a role in neurite outgrowth and axonal guidance[54,55]. The GABAergic neuron 2 subcluster is more abundant in the Xiang-Tanaka and Arber models; these cells exhibit relatively higher expression of neural progenitor markers *SOX4* and *SOX11,* suggesting these are relatively immature neurons as well[56] (Figure S2B-C). GABAergic neuron subclusters 3 & 4, most abundant in the Bagley and Arber models, have robust expression of *GAD1* and *GAD2* along with higher expression of the striatal marker *ARPP21*, suggesting these clusters most closely recapitulate MSNs (Figure S2B-C). Interestingly, Rudbaugh1 is the only model generating GABAergic neuron subcluster 5 with as yet unclear physiological origins, characterized by higher levels of *ARPP21, LAMP5,* and *GRM5.* These results suggest the Bagley and Arber models have the highest percentages of MSN-like GABAergic neurons and may therefore be the best current 3D and 2D models respectively for modeling the striatum. This could be further tested by assessing the relative abundance of MSN marker genes in GABAergic neurons; however, due to limitations in scRNAseq sequencing depth it is challenging to detect the lowly expressed *DARPP32 (PPP1R1B), DRD1,* and *DRD2* transcripts[43] (Figure S2D).

We therefore assess the expression of striatal neuron markers that are known to be more abundantly expressed: *ARPP21*, *CTIP2 (BCL11B)*, and *FOXP1* (Figure 2G). Reassuringly, GABAergic neurons in the Bagley model collectively express these genes at levels higher than the other 3D models (Figure 2G). The Arber model expresses elevated levels of *ARPP21*; however, it does not show higher expression of *BCL11B* and *FOXP1* relative to the other 2D models. Nicoleau and Fjodorova have relatively fewer cells in GABAergic neuron subclusters 3 and 4 but higher levels of *BCL11B* and *FOXP1*. Thus, it is difficult to conclude which 2D model generates the most MSN-like neurons mimicking the striatum. Overall, this analysis reveals that all current 3D and 2D models exhibit considerable heterogeneity, suggesting further work developing differentiation or sorting protocols is required if more homogeneous systems are desired; however, of those tested here, the Bagley model most closely mimics the striatum, and we therefore use it in the following studies with substances of abuse.

Cell type specific differential gene expression responses to dopamine, cocaine, and morphine

Cerebral organoids could provide a compelling model system for studying transcriptional responses to substances of abuse due to the presence of multiple cell types present during development and their relative robustness in culture compared to 2D systems[22,35,57–60]. However, before they can be effectively used as *in vitro* models, further characterization is needed to establish baseline responses to these external stimuli[61,62]. We elect to characterize transcriptomic responses to dopamine, cocaine, and morphine here specifically because of their known relevance to the developing and mature striatum. In particular, MSNs are exposed to dopamine from a relatively young age[63], and dopamine regulates cell cycle and proliferation in the developing ventral forebrain in E13 mice[63–65] in addition to its role as a neurotransmitter. Cocaine's effects in neurons are at least partly mediated through dopamine, driven by increasing the amount dopamine in synaptic clefts by blocking presynaptic reuptake through the dopamine transporter protein[66]. Morphine elicits responses in GABAergic neurons by binding to μ-opioid receptors[5], while opioid receptors are also found on multiple other cell types in the developing brain including progenitors and glia[67,68].

There are many experimental configurations possible to explore. We focus here on probing three: the effect of dopamine on forebrain organoids, as it is a primary presynaptic neurotransmitter for striatal MSNs; whether cocaine impacts MSNs in a manner distinct from direct dopamine treatment when in the presence of DNs in forebrain-midbrain assembloids, as the canonical understanding is that cocaine inhibits

dopamine reuptake by DNs; and how morphine affects cells in forebrain organoids and assembloids. To address these questions, we expose Bagley forebrain organoids to physiologically relevant concentrations of dopamine or morphine, and Bagley-Rudibaugh2 forebrain-midbrain assembloids to cocaine and morphine (Figure 3A). We then perform an in-depth scRNAseq analysis and comparison of five cell types: GABAergic neurons, Glutamatergic neurons, Interneurons, Progenitors, and Radial Glia on their transcriptomic responses to all four conditions. Astrocytes, oligodendrocytes, and mesenchymal cells are excluded as no genes crossed the DEG threshold due to their low cell counts (Figures 3, S3, Supplemental Excel File 1).

Our analysis of cell type specific differentially expressed genes (DEGs) relative to our ascorbic acid dosed vehicle controls reveal, somewhat surprisingly, that there are fewer DEGs in the GABAergic and Glutamatergic neurons compared to the Interneurons, Progenitors, and Radial Glia (Figures 3B, S3A). Thus, the effects of these compounds on transcriptomes may be more diverse than expected. Indeed, when visualizing the overlap of DEGs between cell types there are very few common DEGs, and this pattern holds for all compound treatments (Figure 3C, Supplemental Excel File 2). Similarly, when assessing each cell type and their responses to each compound, there are very few common DEGs between compound treatments (Figure S3B, Supplemental Excel File 2). These suggest that each compound has relatively distinct effects from each other and that different cell types respond distinctly to the same compounds as well. Interestingly, this distinctiveness is observed even between similar cells from Bagley organoids and Bagley-Rudibaugh2 assembloids in response to morphine (Figure S3C). This suggests the nature of the organoids/assembloids themselves influences the transcriptomic response. A broader composition comparison suggests different proportions of the eight unique cellular subtypes in Bagley organoids versus Bagley-Rudibaugh2 assembloids, which is not entirely unexpected (Figure 3D). In addition, cells from each of the five cell types, while generally clustered together on UMAP plots, exhibit some differences between the organoids and assembloids, and may explain their distinct responses to the tested compounds (Figure S3D). Ideally, we would perform subtype specific differential gene expression rather than identifying DEGs between the five broader cell type classes. However, we are unable to do this due to limitations in the number of cells in each individual cluster.

Gene set enrichment analysis of cell type specific responses to dopamine, cocaine, and morphine

To next identify the nature of the cell type specific responses to each distinct compound, we perform gene set enrichment analysis (GSEA) on the cell type specific DEGs following drug exposure and identify the top pathways and upstream regulators (Figure S4, Supplemental Excel File 3). Several cell types show no or very few differentially expressed pathways or regulators following compound exposure, including many of the GABAergic neurons to all compounds and most of the cell types to dopamine. However, while each cell type seemingly shows a unique transcriptional response to each compound, there are some common broader trends. For example, among the 20-cell type specific analyses (5 cell types, 4 conditions each), several regulated pathways are identified multiple times including cellular responses to external stimuli along with oxidative phosphorylation and synapse formation (Figure 4A). The most common cellular response pathway is eIF2 signaling, followed by PI3K, CREB, and mTOR signaling. This trend applies to all five cell types, suggesting the immediate responses to the compounds work through similar pathways.

Thorough investigation of each of the 20-cell type-specific analyses reveals several responses that suggest a need for further investigation at a higher read depth. In this study, we highlight three transcriptional responses that exhibit a relatively higher number of differentially expressed genes (DEGs) and activate genes and pathways previously described in mice: the Interneuron response in Bagley-Rudibaugh2 assembloids to morphine, the Progenitor response in Bagley-Rudibaugh2 assembloids to

cocaine exposure, and the response in glutamatergic neurons in Bagley organoids to morphine exposure. Interneurons in the Bagley-Rudibaugh2 assembloids exposed to morphine show downregulation of the synaptogenesis signaling and synaptic long term potentiation pathways (Figure S4). Within these pathways we observe downregulation of *CAMKIIA*, a gene previously linked with prenatal morphine exposure in mice; along with downregulation of multiple genes associated with *BDNF* expression, a gene similarly linked with prenatal morphine exposure[15,69,70] (Figure 4B). Progenitors in Bagley-Rudibaugh2 assembloids exposed to cocaine exhibit activation of the stress response eIF2 and GP6 signaling pathways which regulate proliferation and cell cycle among others (Figure S4). In addition, multiple collagen genes are upregulated (Figure 4C). Collagen accumulation has not been previously linked with cocaine exposure, but the ECM plays an important, if understudied, role in neurodevelopment and in stress response and neuroplasticity[71]. Cocaine causes premature neural differentiation in early neural progenitors through oxidative stress mediated eIF2 signaling and it is possible this stress response also triggers increased expression of collagen proteins as a byproduct, although further testing is required to confirm this[72,73]. The glutamatergic neurons in Bagley organoids exposed to morphine exhibit upregulation of both the synaptogenesis and reelin signaling pathways; the top upregulated DEGs include *GRIN1* and multiple MAP kinases, suggesting a MAPK mediated pathway that may ultimately lead to regulation of synapse formation (Figure S4, Figure 4D)[74]. The increase in synaptic connections following opioid exposure is unique to glutamatergic neurons in mice models; suggesting organoids may be able to recapitulate this cell-type specific phenotype[69]. Overall, identification of cell type specific DEGs and pathway analysis reveals both some common trends and specific transcriptional responses to dopamine, cocaine, and morphine.

Bulk analysis reveals roles for eIF2 and TGF-β signaling

A major limitation of scRNAseq is transcript capture efficiency and read depth per cell which limits the ability to identify cell type specific DEGs. However, the total reads from scRNAseq samples can also be aggregated and analyzed in bulk. This approach sacrifices single cell resolution in exchange for read depth and could provide a deeper understanding of how these models respond to each compound, responses that may be originally masked by the sparsity of scRNAseq data.

Taking this approach, the compound treated samples are compared to their vehicle controls in bulk (Figure 5, Figure S5). Among the top DEGs across all four treatment conditions: Bagley Dopamine, Bagley Morphine, Bagley-Rudibaugh2 Morphine, Bagley-Rudibaugh2 Cocaine, we observe multiple genes related to immune (*NFIA* and *NFIB*) and stress (*HSP90* and *NRFB1*) responses (Figure S5A-B), matching what is seen in the cell specific analysis. Acute drug exposure is known to alter neuroimmune responses *in vivo*, leading to cellular reactions including cytokine signaling, alterations in metabolic cycles, and even cellular apoptosis[75,76]. These phenotypes have been investigated both in mice and cell cultures; and recent work shows organoids can model neuroinflammation when exposed to acute methamphetamine; however, similar responses to cocaine and morphine have not been previously described in cerebral organoids[22,77]. Thus, we sought to identify what transcriptional pathways may be modulating this immune stress response. Using GSEA for all four treatment conditions, we observe upregulation of the aryl hydrocarbon receptor signaling pathway, which regulates the metabolism and transcriptional response to xenobiotics (Figure 5A).

Interestingly, the transcriptional response to cocaine was the most distinct. In the dopamine and morphine treated samples, we observe the downregulation of the eIF2 Signaling pathway, which is not downregulated in the cocaine treated organoids (Figure 5A). Instead, organoids exposed to cocaine exhibit multiple stress response pathways related to the cell cycle and proliferation including the ERK and AKT pathways, also previously linked to exposure to substances of abuse in the striatum[74,78,79]. Many of these

pathways are linked to TGF-β signaling, which has been implicated in neurodevelopment and potentially responses to prenatal drug exposure[80–83]. In addition, we observe predicted upregulation of multiple fibrosis signaling pathways (Figure 5A). Central nervous system fibrosis has been reported following exposure to unknown pathogens; and results in an increase in ECM deposition[84]. This finding further supports a role for TGF-β signaling as it holds a critical role in regulating the ECM during neurodevelopment[81]. This also provides an explanation for the upregulation of collagen proteins observed in Progenitor cells exposed to cocaine (Figure 4C).

eIF2 functions as a stress signaling pathway which regulates global RNA translation, and previous work has demonstrated morphine and dopamine cause ROS mediated ER stress, ultimately leading to the expression of ER stress kinase gene *(PERK)*[85–87]. This in turn phosphorylates the eIF2α protein causing a cascading effect ultimately leading to a global reduction in RNA translation. We observe *PERK (EIF2AK3*) upregulated in the dopamine and morphine treated samples, suggesting they both contribute to ER stress leading to downregulation of eIF2 signaling (Figure 5B). In addition, all three conditions show the downregulation of multiple eIF2 pathway related genes including eiF2B, a known target for p-eif2α[88]; further supporting these compounds may be causing an ER-stress response acting through the eIF2 signaling pathway (Figure S5C). Taken together, this response suggests morphine exposure and potentially increased synaptic dopamine in the developing brain could lead to an immune regulation response and an ER regulated decrease in eIF2 Signaling. For cocaine exposure, further analysis reveals activation of multiple MAPKKK genes, indicating TGF-β could be potentially working through the ERK signaling pathway[74] (Figure 5A,C). We also observe the upregulation of multiple ECM related genes including *SPARC, CCN1* and *CCN2* and the matrix metalloprotease genes *MMP2* and *MMP14* (Figure 5D), along with downregulation of genes linked with proliferation (*SOX4*, *DSP*, *HDAC4*, and *EZH2*). This suggests cocaine may affect the cytoarchitecture of developing neurons in cerebral organoids, and this response is potentially mediated by the TGF- β pathway[89,90] (Figure 5D).

Discussion

We have established hPSC differentiation protocols for generating striatal and VTA midbrain neurons by modifying the Lancaster whole brain organoid protocol[34]. The Wnt and BMP pathways were stimulated to make striatal organoids and the Wnt, SHH, and FGF pathways were stimulated to generate midbrain organoids. The resultant organoids express key markers of striatal and VTA neurons, respectively, at both D30 and D90. This demonstrates the whole brain organoid protocol can be modified to generate regionally specified organoids. These organoids share a common maturation media after D25, which allows for their fusion in the same media.

While, to our knowledge, this is the first time the presence of DARPP32+ striatal neurons have been confirmed in cerebral organoids, previous groups have generated ventral forebrain organoids, and there are numerous 2D protocols as well as a biomaterial-driven model[91] for generating DARPP32+ striatal neurons. These models were developed by manipulating different morphogen concentrations to achieve neural differentiation, indicating there are multiple methods for generating striatal neurons *in vitro*. While each method generates some striatal neurons, and the literature often assumes a strong level of homogeneity in downstream analyses, our direct comparisons and composition analysis shows significant heterogeneity exists in all 2D and 3D protocols. Only a fraction of cells in all models are positively identified as GABAergic neurons. Only a fraction of those cells could be positively identified as striatal-like neurons, while other subtypes of GABAergic neurons express markers for relatively immature GABAergic neurons or markers for both GABAergic and Glutamatergic neurons. The remaining cells include several different cell types including undifferentiated progenitors, astrocytes, and radial glia. Together, this shows the composition differences between these model systems are relatively

small, and none of these models exhibit a similar composition to the adult *in vivo* striatum but may better mimic the developing striatum. To increase the percentage of DARPP32+ neurons *in vitro* will require significant improvements in stem cell differentiation, or better methods for sorting out the neurons of interest without causing excessive cellular stress.

From another perspective, cellular heterogeneity within organoids can present advantages in efficiently assessing how different cell types respond to external stimuli and providing a more native microenvironment. Recent work has begun using organoid models to study responses to substances of abuse and demonstrated they are able to recapitulate several relevant phenotypes[22,57,60]. For example, Kindberg and colleagues recently demonstrated that cortical organoids exposed to cocaine exhibit an ROS driven cellular response that contributes to premature neural differentiation[92]. Our cell specific analysis also indicates each cell type exhibits differential gene expression following exposure to multiple substances of abuse. Reassuringly, GSEA of the cell type specific responses suggest many of the biological processes observed match what is seen in mouse models, including a neuroinflammatory response to morphine and downregulation of synaptogenesis and synaptic signaling in GABAergic neurons and interneurons following cocaine and morphine exposure (Figure S4, Figure 5A)[22,35,77,93]. Recent work has also suggested that cocaine causes an anti-inflammatory response in the striatum, and one role of TGF-β is an anti-inflammatory cytokine[94]. Cocaine may cause a similar response in cerebral organoids and represents another avenue for further investigation. Among the transcriptional responses not discussed in the results section are the Progenitor response to morphine in Bagley organoids and the GABAergic neuron response to morphine in both Bagley organoids and Bagley-Rudibaugh2 assembloids. DEGs in these cell types are linked with AMPA and NMDA receptors, both of which are linked with prenatal morphine exposure, suggesting another phenotype of interest, and possibly indicating these Progenitor cells are relatively immature neurons[15,76].

We identified a novel role for TGF-β signaling in response to cocaine exposure, and for eIF2 signaling following morphine and dopamine exposure through bulk differential gene expression analysis. Both pathways hold critical roles in neurodevelopment, suggesting mechanisms by which prenatal drug exposure could have adverse effects on development. It could be interesting to further explore the apparent dissimilarity between the morphine treated assembloids from the morphine treated forebrain organoids. Both models induced down regulation of eIF2 signaling; however, the cell type specific DEGs show little overlap between the two organoid models, and indeed the morphine treated assembloids show higher DEG overlap with the cocaine treated assembloids (Figure S4B). One possible explanation is the slight compositional difference between Bagley organoids and Bagley-Rudibaugh2 assembloids. This also highlights the importance of conducting detailed pathway analysis when the overall read depth for cells is low, as individual gene expressions may exhibit variability. Altogether, this work provides novel insights into and baseline transcriptomic responses of hPSC derived cerebral organoids as brain region and cell type specific models for research on substance abuse and prenatal exposure.

Materials and Methods

hESC Cell Lines

H9 and H1 hESCs (WA09 and WA01; WiCell) were grown in E8 media (Thermo Fisher Scientific) in 6 well culture dishes (Greiner Bio-One) coated with 0.5µg/mL Vitronectin (Thermo Fisher Scientific). Cells were passaged every 3-5 days as necessary using 0.5mM EDTA (Thermo Fisher). All staining and qPCR experiments included in Figure 1 were carried out in H1 and H9 stem cells. Due to cost limitations, all sequencing experiments were limited to H1 stem cells.

Organoid Cultures

The Xiang-Tanaka, Bagley, Monzel, an d Lancaster protocol organoids were grown as previously described[25,32,34,45]. The Rudibaugh midbrain and forebrain organoids were generated by modifying the Lancaster whole brain organoid protocol. Stem cells were grown to 75% confluency before dissociation into a single cell suspension using EDTA and Accutase (Fisher). 9,000 cells were plated into a low attachment U-bottomed 96 well plate(VWR) in hESC media supplemented with 50µM Y-27632(LC Labs) and 4ng/mL β-FGF(Thermo Fisher). hESC media contained DMEM-F12(Gibco), 20%v/v knockout serum replacement (Thermo Fisher), 3% v/v fetal bovine serum(Corning), 1% v/v MEM-NEAA(VWR), 1% v/v Glutamax(Gibco) and 7µL/L β-mercaptoethanol(Amresco). After 48 hours, half of the media was replaced with hESC media containing Y-27632 and β-FGF. After another 48 hours, half the media was again removed and replaced with hESC media without Y-27632 and β-FGF. On D6, organoid media was replaced with neural induction media supplemented with 50µg/mL heparin (Sigma). Bagley organoid media was further supplemented with 1µM of SAG(Sigma) and 2.5µM of IWP-2(Stemcell Technologies). Rudibaugh2 organoid media was supplemented with 100ng/mL SHH(VWR) and 2µM purmorphamine (VWR). Neural induction consisted of DMEM-F12, 1% v/v N2 supplement (Thermo Fisher), 1% v/v MEM-NEAA, and 1% v/v Glutamax. After 48 hours, 50% of the neural induction was replaced with fresh neural induction media. Bagley organoid media was again supplemented with heparin, IWP2, and SAG. Rudibaugh1 organoid media was supplemented with heparin; and Rudibaugh2 organoid media was supplemented with SHH and purmorphamine. On D10, neural induction was again changed with the same conditions as D8.

On D12, Bagley, Rudibaugh1, and Rudibaugh2 organoids were removed from the 96 well plates and embedded in Matrigel (Corning) as previously described[34]. Dimples were placed in Parafilm, and one organoid was transferred into each dimple using a cut 200µL pipet tip. 30µL of Matrigel was placed around the organoid and allowed to solidify at 37C for 30 minutes. The embedded organoids were then removed from the Parafilm and placed in a deep bottom 10cm plate (VWR) in COD – vitamin A media. The Rudibaugh forebrain organoid media was supplemented with 100ng/mL of DKK1(Peprotech), and the Rudibaugh midbrain organoid media was supplemented with 100ng/mL SHH, 2µM purmorphamine, and 3µM CHIR99021(Reagents Direct). COD – vitamin A media consisted of 50:50 DMEM-F12: Neurobasal (Gibco) mixture, 0.5% v/v N2 supplement, 1% v/v Glutamax, 0.5% v/v MEM-NEAA, 1% B27 supplement w/o vitamin A (Thermo Fisher), 1% v/v Penicillin/Streptomycin(VWR), 3.5µL/L β-mercaptoethanol, and 12.5µL/L 4mg/mL Insulin(). On D16, the media was replaced with COD + vitamin A media; which has the same components except the B27 w/o vitamin A is replaced with B27 supplement with vitamin A (Thermo Fisher) and placed on an orbital shaker (Thermo Fisher) rotating at 70rpm. The Rudibaugh forebrain organoid media was supplemented with 100ng/mL of DKK1 and the Rudibaugh midbrain organoid media was supplemented with 3µM CHIR99021 and 100ng/mL FGF-8(Peprotech). On D20, organoid media was replaced with fresh COD + vitamin A media. Rudibaugh1 organoid media was supplemented with 25ng/mL Activin A (R&D Systems) and Rudibaugh2 organoid media was

supplemented with 100ng/mL FGF-8. On D24, media was changed, and Rudibaugh1 organoid media was supplemented with 25ng/mL Activin A. After D24, COD + vitamin A media was changed every 5-7 days as necessary until organoids reached desired timepoints.

Assembloids

Organoid fusion assembloids were generated as previously described[32,45]. Briefly, one D25 midbrain and one D25 forebrain organoid were placed in a deep well V-bottomed 96 well plate (VWR) with 2mL of COD+vitamin A media; the plate was placed on the orbital shaker. The media was carefully changed after 48 hours, and after 96 hours organoid fusions were removed with a cut 1000µL pipette tip. Approximately 60% of organoids successfully formed fusion assembloids within 96 hours, those that were not successful were placed back in the V-bottomed plate and given another 96 hours to fuse. Assembloids were placed in 10cm plates and kept stationary for a further 48 hours before being placed back on the orbital shaker.

Cryosectioning and Immunohistochemistry

Tissues were fixed in 4% paraformaldehyde (Sigma) for 15 minutes at 4C followed by 3, 10-minute PBS washes (Gibco). Tissues were placed in 30% sucrose overnight at 4C and then embedded in 10% gelatin/7.5% sucrose (Sigma). Embedded tissues were flash frozen in an isopentane (Sigma) bath between −50 and −30C and stored at -80C. Frozen blocks were cryosectioned (Thermo Fisher) to 30-µm. For immunohistochemistry, sections were blocked and permeabilized in 0.3% Triton X-100 (Sigma) and 5% normal donkey serum (VWR) in PBS. Sections were incubated with primary antibodies in 0.3% Triton X-100, 5% normal donkey serum in PBS overnight at 4C. Sections were then incubated with secondary antibodies in 0.3% Triton X-100, 5% normal donkey serum in PBS for 2 hours at RT, and nuclei were stained with 300nM DAPI (Invitrogen). Slides were mounted using ProLong Antifade Diamond (Thermo Fisher).

Images were taken using a Nikon AR confocal laser scanning microscope (Nikon). All samples within quantification experiments were imaged using the same laser intensity settings using the 10X objective. Quantifications were performed manually in FIJI. Organoid protocol names were first removed, and the images randomized before quantification to avoid bias. A 25x25 grid was overlaid over the image and each grid was manually counted as MAP2+ if over 75% of the region present had MAP2 axons. The images were then remeasured, and regions were considered DARPP32+ if over 50% of the MAP2+ cells appeared to be DARPP32+. For each condition, 4 independent replicates with 3 organoids per replicate were collected and measured.

Real Time Quantitative PCR

Organoids were washed 3 times in ice cold PBS. Matrigel was dissolved by incubating the organoids in chilled Cell Recovery Solution (Corning) for 1 hour at 4C. The dissolved Matrigel was removed by rinsing 3 times in cold PBS. Total RNA was isolated using Direct-zol RNA MicroPrep Kit (Zymo Research) according to the manufacturer's protocol. RNA samples were collected in 2mL RNAse-free tubes and chilled on ice throughout the procedure. cDNA synthesis was performed using 1µg of total RNA and the iScript Reverse Transcription Kit (BIO-RAD) according to the manufacturer's protocol. Real time PCR was performed using the SYBR Green Supermix (BIO-RAD) according to the manufacturer's protocol. Gene expression was compared to the reference genes GAPDH and ΔΔCq values were found by comparing against undifferentiated stem cell controls. For each qPCR condition, 5 independent biological replicates of 2-3 organoids per replicate were collected.

Compound Treatment Experiments

D90 Bagley organoids and Bagley-Rudibaugh2 assembloids were treated with either a physiologically relevant dose of 1µM dopamine, 3µM cocaine (NIDA Drug supply program), or 13µM of morphine (NIDA Drug Supply Program), or an ascorbic acid control. Organoids were kept exposed to compounds for 1 hour before removal and immediate dissociation and fixation according to manufacturer's protocols. 7-10 organoids were used for each condition.

Dissociation and Library Preparation for Single Cell Sequencing

To obtain a single cell dissociation, the papain dissociation kit was used according to the manufacturer's protocols (Worthington). Briefly, 2-3 organoids were initially broken into smaller pieces using a sterile razer before dissociation in papain solution. The cells were broken up further by gently pipetting using a 1000µL pipette.

Barcoding and library preparation of single cell suspensions was performed according to the manufacturer's protocols (SplitBio). The cells were fixed and lysed, before multiple rounds of barcoding and cell measurements were employed to ensure the cells were in a uniform single cell suspension and each cell was given a unique barcode. Barcoded RNA sequences were shipped on dry ice before being sequenced on an Illumina HiSeq 4000x150bp at a depth of 50,000 reads per cell(Illumina Biosciences).

Data Processing for Single Cell Sequencing

Raw sequencing data was preprocessed with splitp to pair oligo-dT primer and random hexamer barcodes used in the initial round of barcoding. A splici (spliced + intron) index was created using salmon (v1.7.0) using human GENCODE v39 and hg38 human reference genome. Sequences were mapped to the splici index using salmon and quantified using alevin fry (v0.5.0). Seurat (v4.1.1) was used to filter, process, and analyze gene expression matrices. The eight sequenced sublibraries were merged into a single Seurat object and reads not matching sample barcodes within a hamming distance of 1 were filtered out. QC filtering was performed removing cells that did not meet the following criteria: Count_RNA > 2000, nFeature_RNA > 1000, mitochondrial percentage < 10%, resulting in 43,844 high-quality cells for analysis. SCTransform was then used to normalize for read depth across cells, scale the data, and find variable features. The mitochondrial mapping percentage was regressed during normalization to remove this confounding source of variation. Principle component analysis (PCA) was performed and an ElboxPlot was generated to determine the number of informative dimensions (50). FindNeighbors, FindClusters, and UMAP dimensionality reduction visualization were performed. Clusters were identified based on the top 10 differentially expressed genes in each cluster, as well as analysis of known marker genes (replace this with however you did your cluster identification).

Cell types for each cluster were determined using previously identified marker genes[45,53,95]. All further downstream analyses were performed in RStudio using the high-performance learning computer available at North Carolina State University. Violin plots and dot plots were generated using open access R packages. The Ingenuity Pathway Analysis tool was used to perform the GSEA analyses presented. Differential gene expression was performed using the FindMarkers function on either all cells in the dosed or vehicle control or a specific cell subtype based on clustering identification. Genes were considered differentially expressed when they had a false discovery rate $q<0.05$, the gene was expressed in over 20% of the cells, and the Log2FC>|0.5|. Z-scores were obtained from the Ingenuity Pathway Software when only significantly differentially expressed genes were studied. Pathways and upstream regulators were considered up or downregulated when they had an adjusted $p<0.05$ and a z-score>|2.0|.

Statistical Analysis

All error bars presented represent a 95% confidence interval assuming a normal distribution. P-values for immunostaining and qPCR experiments were calculated using a 1-way ANOVA test followed by a Tukey-Kramer test. False discovery rates for single cell sequencing were calculated using a Wilcox rank sum test. Information on the number of replicates and organoids per replicate can be found in each experimental procedures section.

References

1. Thompson, L. W. The Dopamine Hypothesis of Schizophrenia. *Perspect. Psychiatr. Care* **26**, 18–23 (1990).
2. Gerfen, C. R. & Bolam, J. P. The Neuroanatomical Organization of the Basal Ganglia. *Handb. Behav. Neurosci.* **20**, 3–28 (2010).
3. Surmeier, D. J., Carrillo-Reid, L. & Bargas, J. Dopaminergic modulation of striatal neurons, circuits, and assemblies. *Neuroscience* **198**, 3–18 (2011).
4. Hyman, S. E., Malenka, R. C. & Nestler, E. J. NEURAL MECHANISMS OF ADDICTION: The Role of Reward-Related Learning and Memory. *Annu. Rev. Neurosci.* **29**, 565–598 (2006).
5. Nestler, E. J. Molecular basis of long-term plasticity underlying addiction. *Nat. Rev. Neurosci.* **2**, 119–128 (2001).
6. Nestler, E. J. Historical review: Molecular and cellular mechanisms of opiate and cocaine addiction. *Trends Pharmacol. Sci.* **25**, 210–218 (2004).
7. Renthal, W. *et al.* Genome-wide Analysis of Chromatin Regulation by Cocaine Reveals a Role for Sirtuins. *Neuron* **62**, 335–348 (2009).
8. Fabio, M. C., Vivas, L. M. & Pautassi, R. M. Prenatal ethanol exposure alters ethanol-induced Fos immunoreactivity and dopaminergic activity in the mesocorticolimbic pathway of the adolescent brain. *Neuroscience* **301**, 221–234 (2015).
9. Walker, B. M. & Koob, G. F. Pharmacological evidence for a motivational role of κ-opioid systems in ethanol dependence. *Neuropsychopharmacology* **33**, 643–652 (2008).
10. Méndez, M., Leriche, M. & Calva, J. C. Acute ethanol administration differentially modulates μ opioid receptors in the rat meso-accumbens and mesocortical pathways. *Mol. Brain Res.* **94**, 148–156 (2001).
11. Renthal, W. & Nestler, E. J. Epigenetic mechanisms in drug addiction and depression. *Princ. Psychiatr. Genet.* 79–89 (2012) doi:10.1017/cbo9781139025997.009.
12. Evans, A. E., Kelly, C. M., Precious, S. V. & Rosser, A. E. Molecular Regulation of Striatal Development: A Review. *Anat. Res. Int.* **2012**, 1–14 (2012).
13. Robinson, T. E. & Kolb, B. Persistent structural modifications in nucleus accumbens and prefrontal cortex neurons produced by previous experience with amphetamine. *J. Neurosci.* **17**, 8491–8497 (1997).
14. Adinoff, B. Contextual determinants of infant affective response. *Harv Rev Psychiatry* **12**, 305–320 (2004).
15. Desai, R. J. *et al.* Exposure to prescription opioid analgesics in utero and risk of neonatal abstinence syndrome: population based cohort study. *BMJ* **350**, h2102 (2015).
16. Nakabeppu, Y. & Nathans, D. A naturally occurring truncated form of FosB that inhibits Fos/Jun transcriptional activity. *Cell* **64**, 751–759 (1991).
17. Feng, J. *et al.* Chronic cocaine-regulated epigenomic changes in mouse nucleus accumbens. *Genome Biol.* **15**, (2014).
18. Nestler, E. J., Barrot, M. & Self, D. W. ΔFosB: A sustained molecular switch for addiction. *Proc. Natl. Acad. Sci. U. S. A.* **98**, 11042–11046 (2001).

19. Taura, J. *et al.* Behavioral control by striatal adenosine A2A-dopamine D2 receptor heteromers. *Genes, Brain Behav.* **17**, 1–11 (2018).
20. Itskovitz-Eldor, J. *et al.* Differentiation of human embryonic stem cells into embryoid bodies compromising the three embryonic germ layers. *Mol. Med.* **6**, 88–95 (2000).
21. Conley, B. J., Young, J. C., Trounson, A. O. & Mollard, R. Derivation, propagation and differentiation of human embryonic stem cells. *Int. J. Biochem. Cell Biol.* **36**, 555–567 (2004).
22. Dang, J. *et al.* Glial cell diversity and methamphetamine-induced neuroinflammation in human cerebral organoids. *Mol. Psychiatry* 9–11 (2020) doi:10.1038/s41380-020-0676-x.
23. Fjodorova, M., Noakes, Z. & Li, M. How to make striatal projection neurons. *Neurogenesis* **2**, 1–6 (2015).
24. Qian, X. *et al.* Brain-Region-Specific Organoids Using Mini-bioreactors for Modeling ZIKV Exposure. *Cell* **165**, 1238–1254 (2016).
25. Monzel, A. S. *et al.* Derivation of Human Midbrain-Specific Organoids from Neuroepithelial Stem Cells. *Stem Cell Reports* **8**, 1144–1154 (2017).
26. Nicoleau, C. *et al.* Embryonic stem cells neural differentiation qualifies the role of Wnt/β-Catenin signals in human telencephalic specification and regionalization. *Stem Cells* **31**, 1763–1774 (2013).
27. Jo, J. *et al.* Midbrain-like Organoids from Human Pluripotent Stem Cells Contain Functional Dopaminergic and Neuromelanin-Producing Neurons. *Cell Stem Cell* **19**, 248–257 (2016).
28. Kele, J. *et al.* Neurogenin 2 is required for the development of ventral midbrain dopaminergic neurons. *Development* **133**, 495–505 (2006).
29. Cambray, S. *et al.* Activin induces cortical interneuron identity and differentiation in embryonic stem cell-derived telencephalic neural precursors. *Nat. Commun.* **3**, (2012).
30. Arber, C. *et al.* Activin a directs striatal projection neuron differentiation of human pluripotent stem cells. *Dev.* **142**, 1375–1386 (2015).
31. Kriks, S. *et al.* Dopamine neurons derived from human ES cells efficiently engraft in animal models of Parkinson's disease. *Nature* **480**, 547–551 (2011).
32. Bagley, J. A., Reumann, D., Bian, S., Lévi-Strauss, J. & Knoblich, J. A. Fused cerebral organoids model interactions between brain regions. *Nat. Methods* **14**, 743–751 (2017).
33. Kelava, I. & Lancaster, M. A. Stem Cell Models of Human Brain Development. *Cell Stem Cell* **18**, 736–748 (2016).
34. Lancaster, M. A. *et al.* Cerebral organoids model human brain development and microcephaly. *Nature* **501**, 373–379 (2013).
35. Lee, C. T. *et al.* CYP3A5 Mediates Effects of Cocaine on Human Neocorticogenesis: Studies using an in Vitro 3D Self-Organized hPSC Model with a Single Cortex-Like Unit. *Neuropsychopharmacology* **42**, 774–784 (2017).
36. Han, J. J. & Han, J. J. FDA Modernization Act 2 . 0 allows for alternatives to animal testing. 1–2 (2023) doi:10.1111/aor.14503.
37. Iannielli, A. *et al.* Reconstitution of the Human Nigro-striatal Pathway on-a-Chip Reveals OPA1-Dependent Mitochondrial Defects and Loss of Dopaminergic Synapses. *Cell Rep.* **29**, 4646-4656.e4 (2019).
38. Fasano, C. *et al.* Dopamine facilitates dendritic spine formation by cultured striatal medium spiny neurons through both D1 and D2 dopamine receptors. *Neuropharmacology* **67**, 432–443 (2013).
39. Friling, S. *et al.* Efficient production of mesencephalic dopamine neurons by Lmxla expression in embryonic stem cells. *Proc. Natl. Acad. Sci. U. S. A.* **106**, 7613–7618 (2009).
40. Schwartz, C. M. *et al.* Stromal factors SDF1α, sFRP1, and VEGFD induce dopaminergic neuron

differentiation of human pluripotent stem cells. *J. Neurosci. Res.* **90**, 1367–1381 (2012).
41. Jo, J. *et al.* Midbrain-like Organoids from Human Pluripotent Stem Cells Contain Functional Dopaminergic and Neuromelanin-Producing Neurons. *Cell Stem Cell* **19**, 248–257 (2016).
42. Zeng, X. *et al.* An in vitro model of human dopaminergic neurons derived from embryonic stem cells: MPP+ toxicity and GDNF neuroprotection. *Neuropsychopharmacology* **31**, 2708–2715 (2006).
43. Conforti, P. *et al.* In vitro-derived medium spiny neurons recapitulate human striatal development and complexity at single-cell resolution. *Cell Reports Methods* **2**, 100367 (2022).
44. Wu, M. *et al.* A Chemical Recipe for Generation of Clinical-Grade Striatal Neurons from hESCs. *Stem Cell Reports* **11**, 635–650 (2018).
45. Xiang, Y. *et al.* Fusion of Regionally Specified hPSC-Derived Organoids Models Human Brain Development and Interneuron Migration. *Cell Stem Cell* **21**, 383-398.e7 (2017).
46. Liu, X. *et al.* Direct reprogramming of human fibroblasts into dopaminergic neuron-like cells. *Cell Res.* **22**, 321–332 (2012).
47. Chinta, S. J. & Andersen, J. K. Dopaminergic neurons. *Int. J. Biochem. Cell Biol.* **37**, 942–946 (2005).
48. Sheng, Y. *et al.* Using iPSC-derived human DA neurons from opioid-dependent subjects to study dopamine dynamics. *Brain Behav.* **6**, 1–13 (2016).
49. Kirkeby, A. *et al.* Predictive Markers Guide Differentiation to Improve Graft Outcome in Clinical Translation of hESC-Based Therapy for Parkinson's Disease. *Cell Stem Cell* **20**, 135–148 (2017).
50. Hospital, C. U. Differentiation of Mesenchymal Stem Cells Into Dopaminergic Neuron-like Cells in vitro 1. **42**, 36–42 (2005).
51. Cho, M. S. *et al.* Highly efficient and large-scale generation of functional dopamine neurons from human embryonic stem cells. 2–7 (2008) doi:10.1073/pnas.0712359105.
52. Hendrickx, M., Van, X. H. & Leyns, L. Anterior-posterior patterning of neural differentiated embryonic stem cells by canonical Wnts, Fgfs, Bmp4 and their respective antagonists. *Dev. Growth Differ.* **51**, 687–698 (2009).
53. Kanton, S. *et al. Organoid single-cell genomic atlas uncovers human-specific features of brain development*. *Nature* vol. 574 (2019).
54. Ojeda, J. & Ávila, A. Early Actions of Neurotransmitters During Cortex Development and Maturation of Reprogrammed Neurons. *Front. Synaptic Neurosci.* **11**, 1–14 (2019).
55. Sanes, D. H., Reh, T. A. & Harris, W. A. *Axon growth and guidance*. *Development of the Nervous System* (2012). doi:10.1016/b978-0-12-374539-2.00009-4.
56. Liu, H. *et al.* High-efficient transfection of human embryonic stem cells by single-cell plating and starvation. *Stem Cells Dev.* **25**, 477–491 (2016).
57. Yao, H. *et al.* Endogenous and exogenous opioid effects on oligodendrocyte biology and developmental brain myelination. *Stem Cell Res.* **86**, 102065 (2021).
58. Savell, K. E. *et al.* A dopamine-induced gene expression signature regulates neuronal function and cocaine response. *bioRxiv* 781872 (2019) doi:10.1101/781872.
59. Badisa, R. B. *et al.* Cellular and molecular responses to acute cocaine treatment in neuronal-like N2a cells: potential mechanism for its resistance in cell death. *Cell Death Discov.* **4**, (2018).
60. Willner, D. *et al.* Short term morphine exposure in vitro alters proliferation and differentiation of neural progenitor cells and promotes apoptosis via Mu receptors. *PLoS One* **9**, 1–11 (2014).
61. Marshall, J. J. & Mason, J. O. Mouse vs man: Organoid models of brain development & disease. *Brain Res.* **1724**, (2019).
62. Koo, B., Choi, B., Park, H. & Yoon, K. J. Past, Present, and Future of Brain Organoid

Technology. *Mol. Cells* **42**, 617–627 (2019).
63. Ohtani, N., Goto, T., Waeber, C. & Bhide, P. G. Dopamine modulates cell cycle in the lateral ganglionic eminence. *J. Neurosci.* **23**, 2840–2850 (2003).
64. Popolo, M., McCarthy, D. M. & Bhide, P. G. Influence of dopamine on precursor cell proliferation and differentiation in the embryonic mouse telencephalon. *Dev. Neurosci.* **26**, 229–244 (2004).
65. Kippin, T. E., Kapur, S. & Van Der Kooy, D. Dopamine specifically inhibits forebrain neural stem cell proliferation, suggesting a novel effect of antipsychotic drugs. *J. Neurosci.* **25**, 5815–5823 (2005).
66. Russo, S. J., Dietz, D. M., Dumitriu, D., Malenka, R. C. & Nestler, E. J. The Addicted Synapse: Mechanisms of Synaptic and Structural Plasticity in Nucleus Accumbens. *Trends Neurosci.* **33**, 267–276 (2011).
67. Tan, K. Z., Cunningham, A. M., Joshi, A., Oei, J. L. & Ward, M. C. Expression of kappa opioid receptors in developing rat brain – Implications for perinatal buprenorphine exposure. *Reprod. Toxicol.* **78**, 81–89 (2018).
68. Stiene-Martin, A. *et al.* Opioid system diversity in developing neurons, astroglia, and oligodendroglia in the subventricular zone and striatum: Impact on gliogenesis in vivo. *Glia* **36**, 78–88 (2001).
69. Boggess, T. *et al.* Alterations in Excitatory and Inhibitory Synaptic Development Within the Mesolimbic Dopamine Pathway in a Mouse Model of Prenatal Drug Exposure. *Front. Pediatr.* **9**, 1–14 (2021).
70. Konijnenberg, C. & Melinder, A. Prenatal exposure to methadone and buprenorphine: A review of the potential effects on cognitive development. *Child Neuropsychol.* **17**, 495–519 (2011).
71. Mohan, V., Edamakanti, C. R. & Pathak, A. Editorial: Role of extracellular matrix in neurodevelopment and neurodegeneration. *Front. Cell. Neurosci.* **17**, (2023).
72. Lee, C. T. *et al.* A mechanism for the inhibition of neural progenitor cell proliferation by cocaine. *PLoS Med.* **5**, 0987–1004 (2008).
73. Martins, S. G., Zilhão, R., Thorsteinsdóttir, S. & Carlos, A. R. Linking Oxidative Stress and DNA Damage to Changes in the Expression of Extracellular Matrix Components. *Front. Genet.* **12**, (2021).
74. Kyriakis, J. M. & Avruch, J. MAP Kinase Pathways. *Compend. Inflamm. Dis.* 892–908 (2016) doi:10.1007/978-3-7643-8550-7_37.
75. Poon, H. F., Abdullah, L., Mullan, M. A., Mullan, M. J. & Crawford, F. C. Cocaine-induced oxidative stress precedes cell death in human neuronal progenitor cells. *Neurochem. Int.* **50**, 69–73 (2007).
76. Nasiraei-Moghadam, S. *et al.* Reversal of prenatal morphine exposure-induced memory deficit in male but not female rats. *J. Mol. Neurosci.* **50**, 58–69 (2013).
77. Yao, H. *et al.* Methadone interrupts neural growth and function in human cortical organoids. *Stem Cell Res.* **49**, 102065 (2020).
78. Zhu, H. *et al.* Akt and its phosphorylation in nucleus accumbens mediate heroin-seeking behavior induced by cues in rats. *Addict. Biol.* **26**, 1–10 (2021).
79. Lu, L., Koya, E., Zhai, H., Hope, B. T. & Shaham, Y. Role of ERK in cocaine addiction. *Trends Neurosci.* **29**, 695–703 (2006).
80. Gancarz-Kausch, A. M. *et al.* Transforming growth factor beta receptor 1 is increased following abstinence from cocaine self-administration, but not cocaine sensitization. *PLoS One* **8**, 1–5 (2013).

81. Edlund, S., Landström, M., Heldin, C. H. & Aspenström, P. Transforming growth factor-β-induced mobilization of actin cytoskeleton requires signaling by small GTPases Cdc42 and RhoA. *Mol. Biol. Cell* **13**, 902–914 (2002).
82. Wrana, J. L. Signaling by the TGFβ superfamily. *Cold Spring Harb. Perspect. Biol.* **5**, (2013).
83. Differentiation, N., Meyers, E. A. & Kessler, J. A. TGF- b Family Signaling in Neural and and Function. 1–26 (2018).
84. Aldrich, A. & Kielian, T. Central nervous system fibrosis is associated with fibrocyte-like infiltrates. *Am. J. Pathol.* **179**, 2952–2962 (2011).
85. Meiser, J., Weindl, D. & Hiller, K. Complexity of dopamine metabolism. *Cell Commun. Signal.* **11**, 1–18 (2013).
86. Cai, Y. *et al.* Regulation of morphine-induced synaptic alterations: Role of oxidative stress, ER stress, and autophagy. *J. Cell Biol.* **215**, 245–258 (2016).
87. Biswas, K., Alexander, K. & Francis, M. M. Reactive Oxygen Species: Angels and Demons in the Life of a Neuron. *NeuroSci* **3**, 130–145 (2022).
88. Cnop, M., Toivonen, S., Igoillo-Esteve, M. & Salpea, P. Endoplasmic reticulum stress and eIF2α phosphorylation: The Achilles heel of pancreatic β cells. *Mol. Metab.* **6**, 1024–1039 (2017).
89. Ercan, E. *et al.* Neuronal CTGF/CCN2 negatively regulates myelination in a mouse model of tuberous sclerosis complex. *J. Exp. Med.* **214**, 681–697 (2017).
90. Singh, D., Srivastava, S. K., Chaudhuri, T. K. & Upadhyay, G. Multifaceted role of matrix metalloproteinases (MMPs). *Front. Mol. Biosci.* **2**, 1–5 (2015).
91. Adil, M. M. *et al.* hPSC-Derived Striatal Cells Generated Using a Scalable 3D Hydrogel Promote Recovery in a Huntington Disease Mouse Model. *Stem Cell Reports* **10**, 1481–1491 (2018).
92. Kindberg, A. A. *et al.* An in vitro model of human neocortical development using pluripotent stem cells: Cocaine-induced cytoarchitectural alterations. *DMM Dis. Model. Mech.* **7**, 1397–1405 (2014).
93. White, F. J. & Kalivas, P. W. Neuroadaptations involved in amphetamine and cocaine addiction. *Drug Alcohol Depend.* **51**, 141–153 (1998).
94. Mews, P. *et al.* Convergent abnormalities in striatal gene networks in human cocaine use disorder and mouse cocaine administration models. *Sci. Adv.* **9**, eadd8946 (2023).
95. Czerniecki, S. M. *et al.* hESC-Derived Thalamic Organoids Form Reciprocal Projections When Fused with Cortical Organoids. *Cell Stem Cell* **21**, 487-497.e7 (2017).

Acknowledgments

Cocaine and morphine were provided by the National Institutes of Drug Abuse (NIDA) as part of their drug supply program. We thank Dr. John Meitzen and Dr. Jeremy Simon for their help and thoughtful insights. We thank the In-Hyun Park research group for answering our questions and providing useful insights on their organoid protocol. We further thank the Park research group for kindly sharing their sequencing data with us and answering our questions. We thank Dr. Zuzana Drobna for providing the fluorescent cell line and all the assistance with our lab. We also thank Dr. Dilara Sen, Dr. Maria Fadri, and Sam Stuppy for their help and support.

Funding:

NIH Avenir Award DP1-DA044359 (AJK)
Ruth L. Kirschstein Research Award F31 DA053128-01 (TPR)

Author contributions:

Conceptualization: TPR, RT, AJK
Wet Lab Experiments: TPR and RT
Upstream Bioinformatic Analysis: CE
Downstream Bioinformatic Analysis: CE, TPR, RT
Writing: TPR and AJK

Competing interests: The authors declare no competing interests.

Data and materials availability: The sequencing data is available at: GSE225497.

Figures and Tables

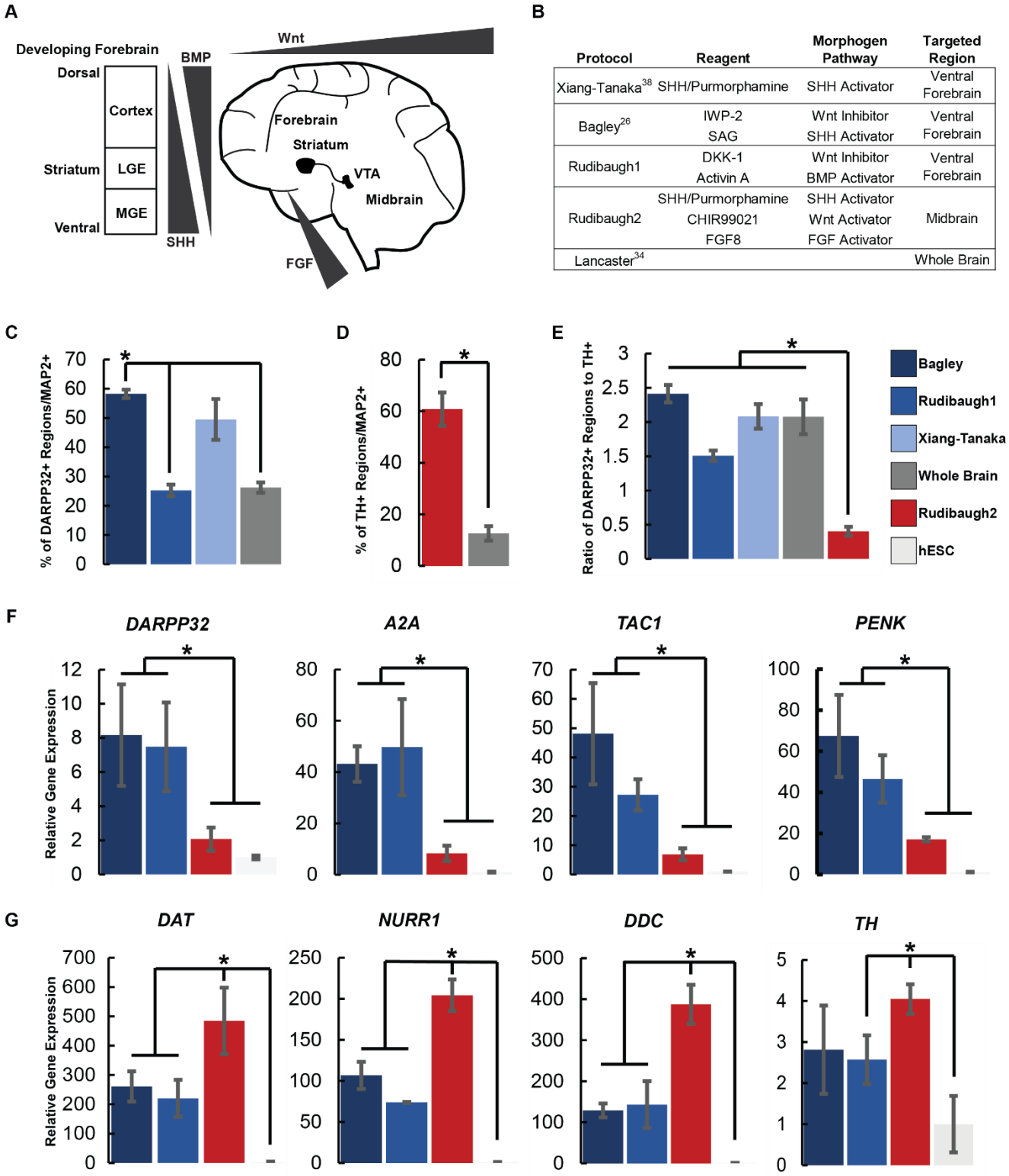

Figure 1. ***Development of striatal and midbrain organoids compatible with early assembloid generation*** **(A)** Morphogen gradients associated with patterning the developing mesolimbic pathway. **(B)** Previously developed 3D forebrain organoid models and new forebrain and midbrain organoid models, with key

patterning factors used, their indicated activities, and targeted regional specifications. **(C)** Immunostaining quantification of D90 forebrain and whole brain organoids. **(D)** Immunostaining quantification of D90 midbrain and whole brain organoids. **(E)** Immunostaining quantification of the ratio of DARPP32+ to TH+ regions in D90 forebrain, midbrain, and whole brain organoids. **(C-E)** Error bars represent 95% confidence intervals for n=4 biological replicates with 3 organoids per replicate. *$p<0.05$, one-way ANOVA with Tukey Kramer post hoc analysis. **(F-G)** RT-qPCR of D90 forebrain organoids, midbrain organoids, and hPSCs for **(F)** MSN markers *DARPP32*, *A2A*, *TAC1*, and *PENK* and **(G)** DN markers *TH*, *NURR1*, *DAT*, and *DDC*. Error bars represent 95% confidence intervals for n=5 replicates with 3 organoids per replicate. *$p<0.05$, one-way ANOVA with Tukey Kramer post hoc analysis.

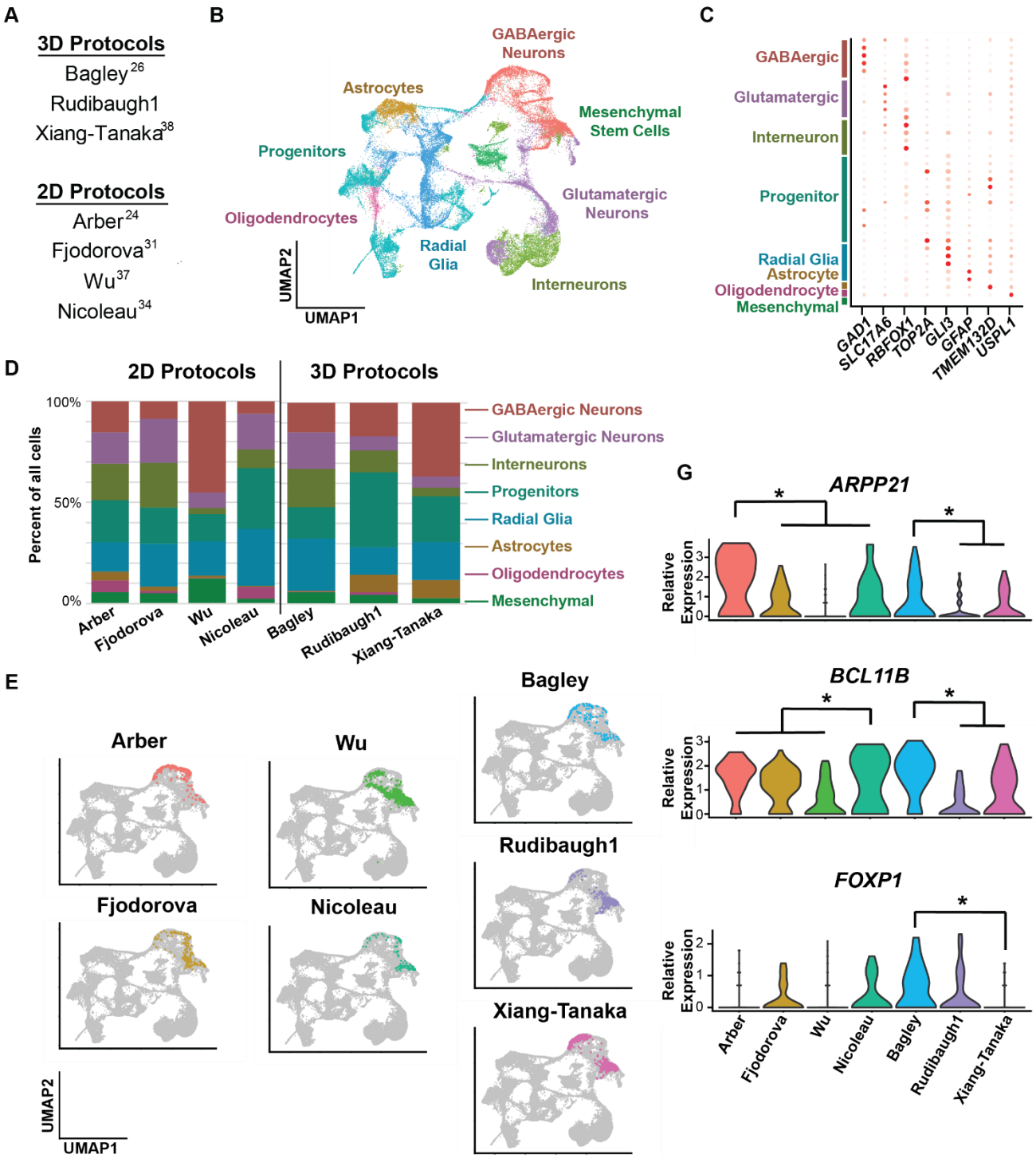
A
3D Protocols
Bagley[26]
Rudibaugh1
Xiang-Tanaka[38]
2D Protocols
Arber[24]
Fjodorova[31]
Wu[37]
Nicoleau[34]
B
GABAergic Neurons
Astrocytes
Mesenchymal Stem Cells
Progenitors
Glutamatergic Neurons
Oligodendrocytes
Radial Glia
Interneurons
UMAP2
UMAP1
C
GABAergic
Glutamatergic
Interneuron
Progenitor
Radial Glia
Astrocyte
Oligodendrocyte
Mesenchymal
GAD1
SLC17A6
RBFOX1
TOP2A
GLI3
GFAP
TMEM132D
USPL1
D
2D Protocols
3D Protocols
Percent of all cells
100%
50%
0%
Arber
Fjodorova
Wu
Nicoleau
Bagley
Rudibaugh1
Xiang-Tanaka
GABAergic Neurons
Glutamatergic Neurons
Interneurons
Progenitors
Radial Glia
Astrocytes
Oligodendrocytes
Mesenchymal
G
ARPP21
BCL11B
FOXP1
Relative Expression
E
Arber
Wu
Fjodorova
Nicoleau
Bagley
Rudibaugh1
Xiang-Tanaka
UMAP2
UMAP1
F
GABAergic Neuron 1
GABAergic Neuron 2
GABAergic Neuron 3
GABAergic Neuron 4
GABAergic Neuron 5

788

Figure 2. ***scRNAseq reveals heterogeneous compositions and distinct enrichments of GABAergic subtypes in seven 3D and 2D striatal models***

(A) Table of the different striatal protocols used in the sequencing experiment. **(B)** UMAP plot shows positions of the 8 different identified cell types. **(C)** Dot plot of select marker genes showing how certain cell types were identified. **(D)** Cell type percentages of the 3 3D organoid protocols and 4 2D protocols show significant heterogeneity. **(E)** UMAP plots show the relative position of the GABAergic neurons in the seven different 2D and 3D culture models. **(F)** UMAP plots show the relative position of the five GABAergic neuron subclusters arranged from most to fewest number of cells. **(G)** Violin plots show GABAergic neurons in Bagley organoids have higher expression of striatal marker genes: *ARPP21*, *BCL11B (CTIP2)*, and *FOXP1* than the GABAergic neurons in the Xiang-Tanaka and Rudibaugh1 models. * false discovery rate $q<0.05$ relative to the other protocols.

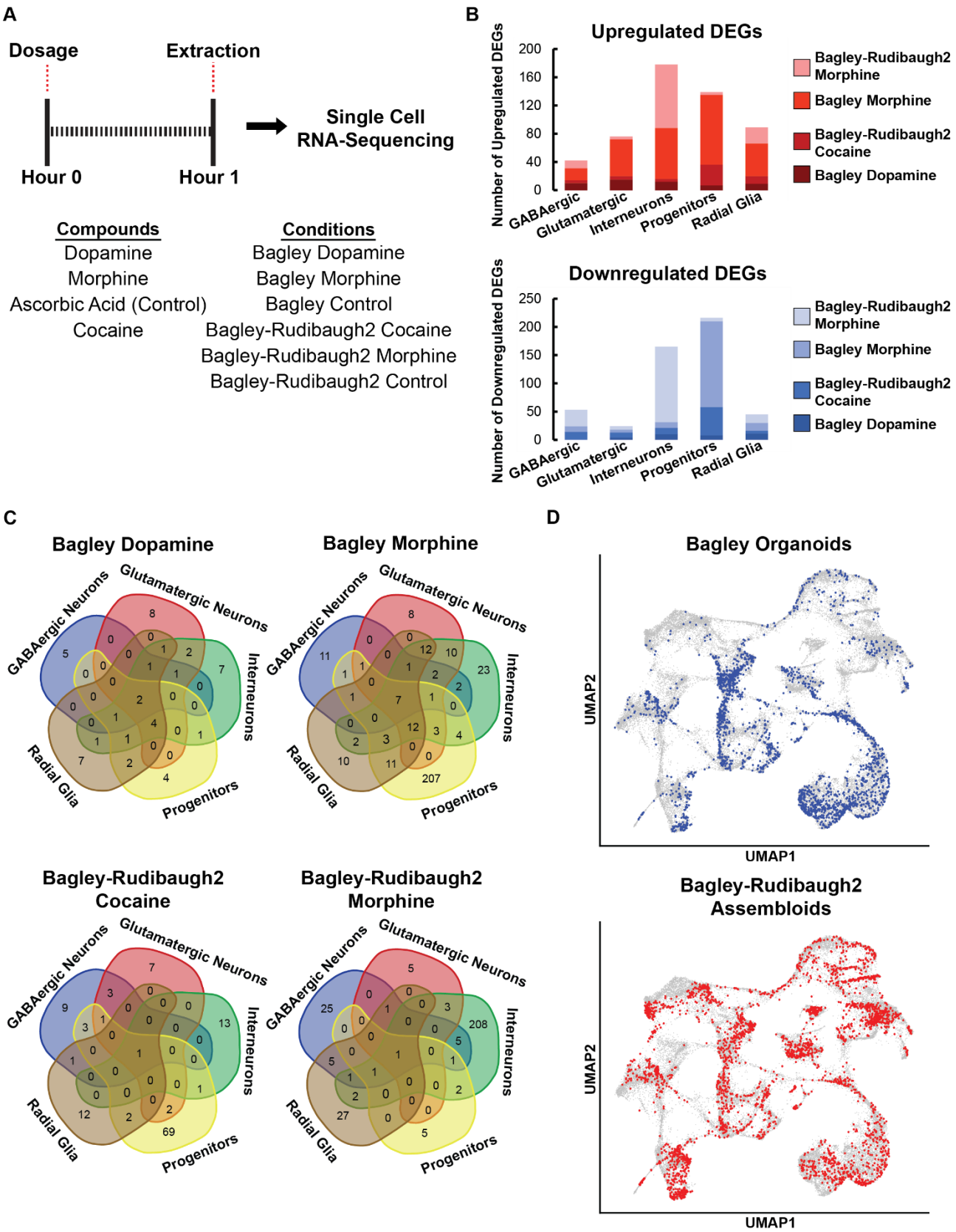
A
Dosage
Extraction
Hour 0
Hour 1
Single Cell RNA-Sequencing
Compounds
Dopamine
Morphine
Ascorbic Acid (Control)
Cocaine
Conditions
Bagley Dopamine
Bagley Morphine
Bagley Control
Bagley-Rudibaugh2 Cocaine
Bagley-Rudibaugh2 Morphine
Bagley-Rudibaugh2 Control
B
Upregulated DEGs
Number of Upregulated DEGs
Downregulated DEGs
Number of Downregulated DEGs
GABAergic
Glutamatergic
Interneurons
Progenitors
Radial Glia
Bagley-Rudibaugh2 Morphine
Bagley Morphine
Bagley-Rudibaugh2 Cocaine
Bagley Dopamine
C
Bagley Dopamine
Bagley Morphine
Bagley-Rudibaugh2 Cocaine
Bagley-Rudibaugh2 Morphine
GABAergic Neurons
Glutamatergic Neurons
Interneurons
Progenitors
Radial Glia
D
Bagley Organoids
Bagley-Rudibaugh2 Assembloids
UMAP1
UMAP2

800

Figure 3. ***Cell type specific differential gene expression to dopamine, cocaine, and morphine***
(A) Schematic of the six different conditions evaluated, the compounds used, and the duration of compound exposure. **(B)** Number of up and downregulated DEGs separated by cell type and condition. DEG defined as log2FC>|0.5|, expression in over 20% of sequenced cells, and false discovery rate q<0.05 relative to ascorbic acid dosed controls. **(C)** Venn diagrams comparing the DEGs across the 5 different cell types keeping the compound regimen constant. **(D)** UMAP plots show the relative positions of all cells from Bagley organoids and Bagley-Rudibaugh2 assembloids.

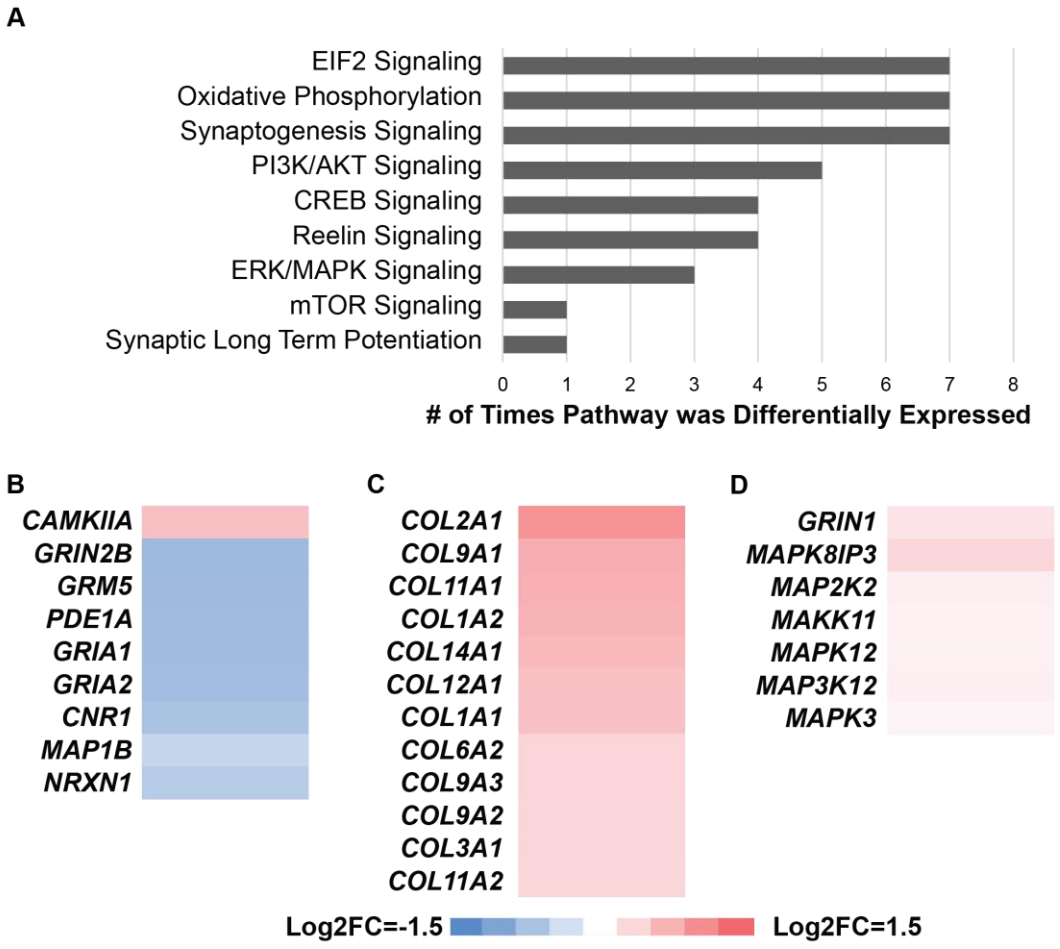

Figure 4. ***Gene set enrichment analysis of cell type specific responses to dopamine, cocaine, and morphine***
(A) Counts of the top activated cell signaling and synapse related pathways based on the 20 unique cell-type specific DGE analyses performed. **(B-D)** Heat maps of differentially expressed genes from **(B)** Interneurons in Bagley-Rudibaugh2 assembloids exposed to morphine. **(C)** Progenitors in Bagley-Rudibaugh2 assembloids exposed to cocaine. **(D)** Glutamatergic neurons in Bagley organoids exposed to morphine. **(B-D)** All genes shown have false discovery rate q<0.05 relative to ascorbic acid dosed controls.

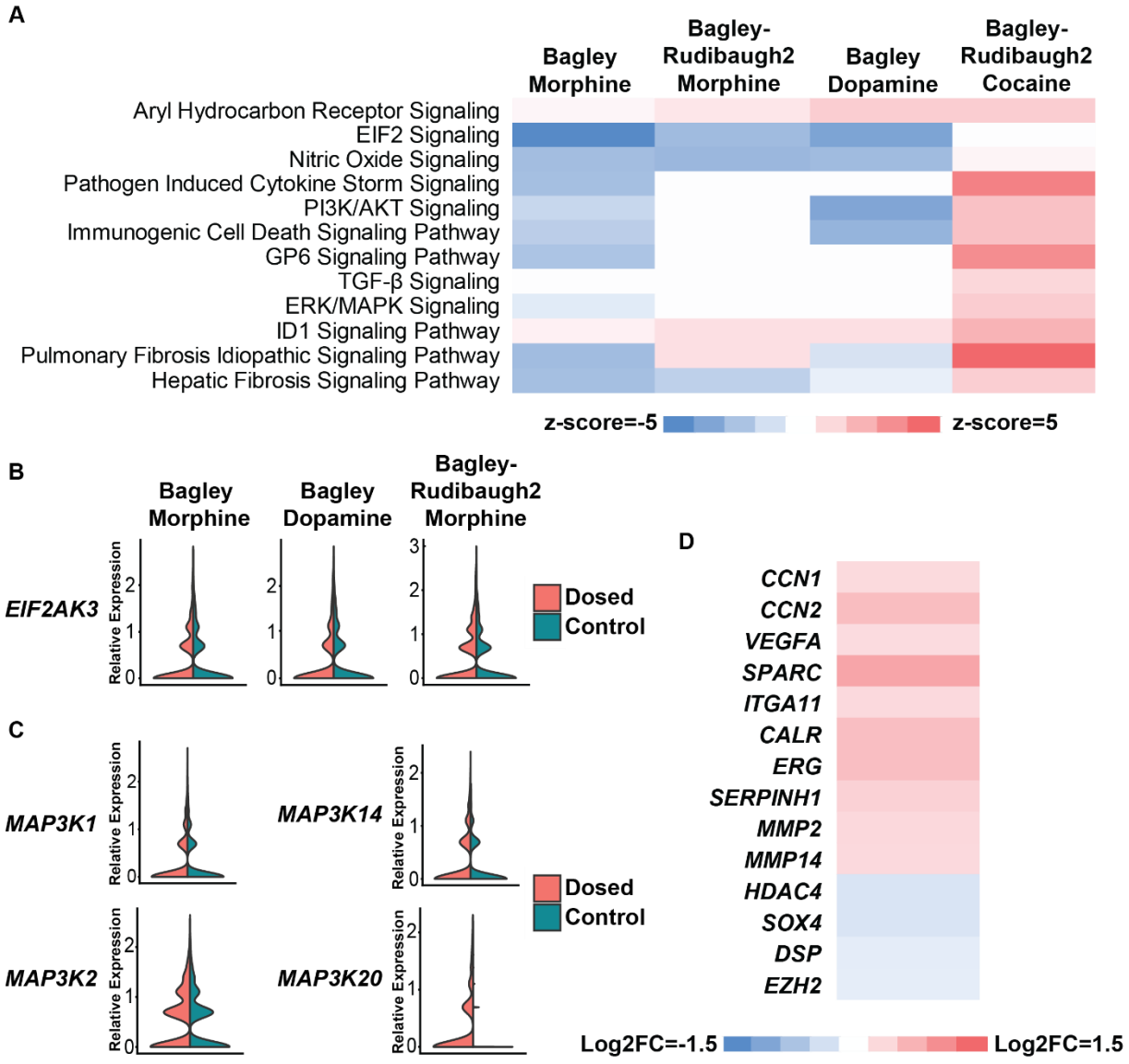

Figure 5. ***Bulk analysis reveals roles for eIF2 and TGF-β signaling pathways***
(A) GSEA shows the Bagley Dopamine, Bagley Morphine, and Bagley-Rudibaugh2 morphine conditions exhibit downregulation of EIF2 Signaling. The Bagley-Rudibaugh2 Cocaine condition exhibits upregulation of TGF-β linked pathways. **(B)** The Bagley Dopamine, Bagley Morphine, and Bagley-Rudibaugh2 morphine conditions show upregulation of the *EIF2AK3* gene linked with ER stress and EIF2 phosphorylation. **(C)** Cocaine dosing causes upregulation of MAPKKK genes in Bagley-Rudibaugh2 assembloids. **(D)** Heat map of select, ECM-related DEGs following cocaine exposure. **(B-D)** All genes shown have log2FC>|0.5|, expression in over 20% of cells, and false discovery rate q<0.05 relative to ascorbic acid dosed controls.

Science Advances
AAAS

Supplementary Materials for

Single cell assessment of human stem cell derived mesolimbic models and their responses to substances of abuse.

Thomas P. Rudibaugh *et al.*

*Corresponding author. Email: ajkeung@ncsu.edu

This PDF file includes:

Figures S1 to S5
Tables S1 to S3

Other Supplementary Materials for this manuscript include the following:

Excel Files S1 to S3

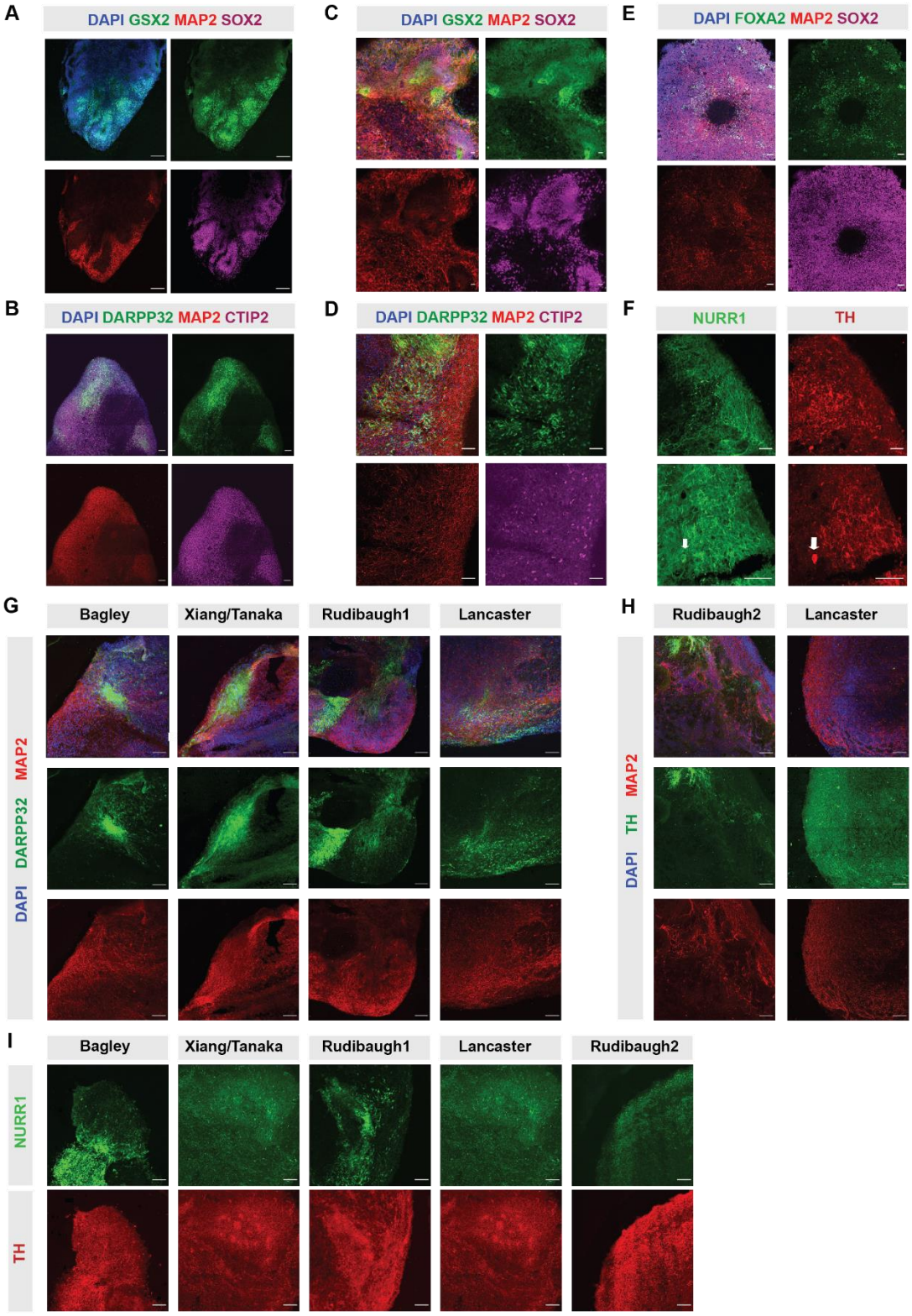
A
DAPI GSX2 MAP2 SOX2
C
DAPI GSX2 MAP2 SOX2
E
DAPI FOXA2 MAP2 SOX2
B
DAPI DARPP32 MAP2 CTIP2
D
DAPI DARPP32 MAP2 CTIP2
F
NURR1
TH
G
Bagley
Xiang/Tanaka
Rudibaugh1
Lancaster
DAPI DARPP32 MAP2
H
Rudibaugh2
Lancaster
DAPI TH MAP2
I
Bagley
Xiang/Tanaka
Rudibaugh1
Lancaster
Rudibaugh2
NURR1
TH

Related to Figure 1; Figure S1: ***Modification of the Lancaster whole brain model to generate forebrain and midbrain organoids***

(A-B) Immunostaining of **(A)** D30 and **(B)** D90 Rudibaugh1 forebrain organoids. **(C-D)** Immunostaining of **(C)** D30 and **(D)** D90 Bagley organoids. **(E)** Immunostaining of D30 Rudibaugh2 midbrain organoids. **(F)** D90 Rudibaugh2 organoids. **(G)** D90 Rudibaugh1, Bagley, and Xiang-Tanaka organoids. **(H)** D90 Rudibaugh2 organoids **(I)** D90 Bagley, Xiang-Tanaka, Rudibaugh1, Lancaster, and Rudibaugh2 organoids.

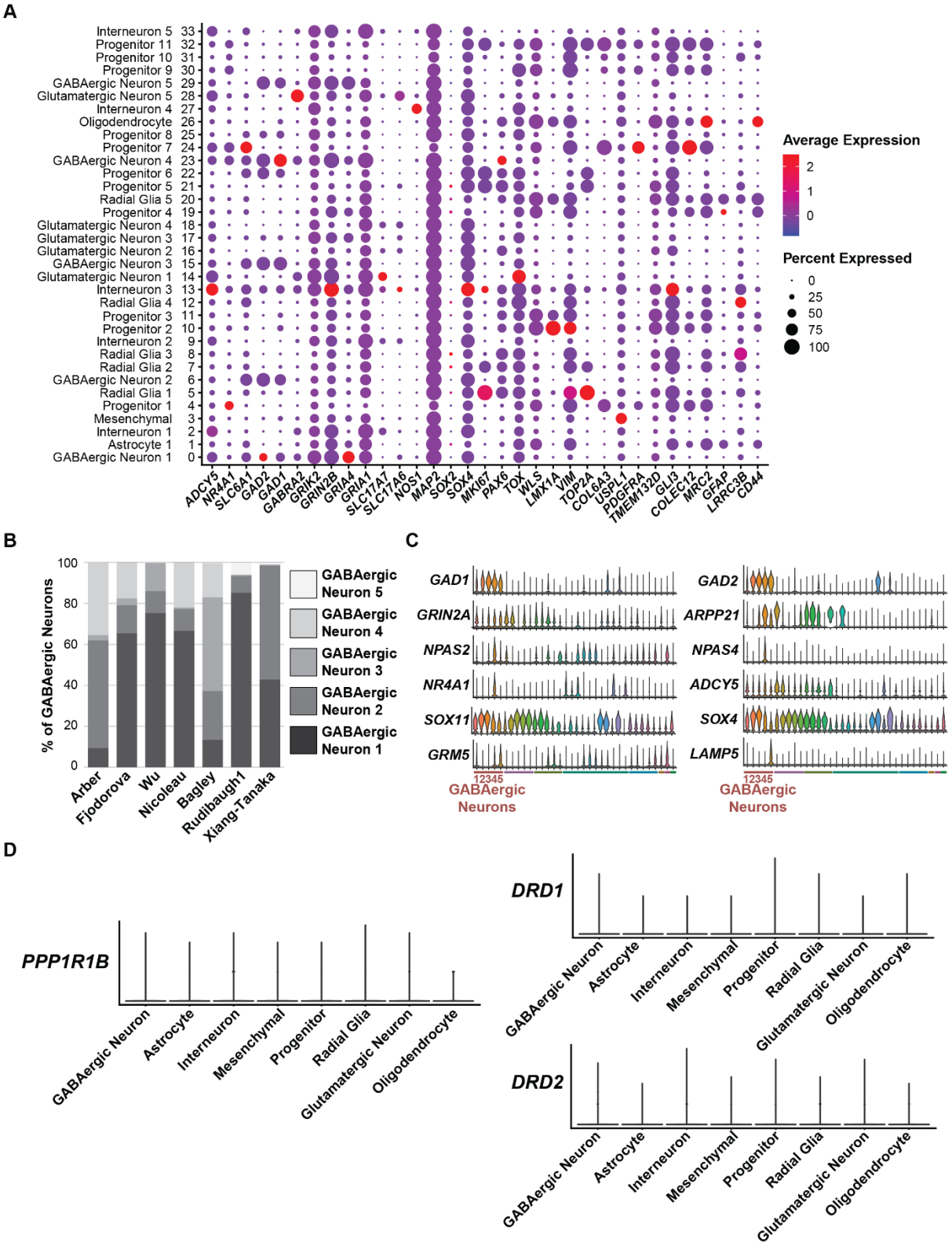
A
Interneuron 5 33
Progenitor 11 32
Progenitor 10 31
Progenitor 9 30
GABAergic Neuron 5 29
Glutamatergic Neuron 5 28
Interneuron 4 27
Oligodendrocyte 26
Progenitor 8 25
Progenitor 7 24
GABAergic Neuron 4 23
Progenitor 6 22
Progenitor 5 21
Radial Glia 5 20
Progenitor 4 19
Glutamatergic Neuron 4 18
Glutamatergic Neuron 3 17
Glutamatergic Neuron 2 16
GABAergic Neuron 3 15
Glutamatergic Neuron 1 14
Interneuron 3 13
Radial Glia 4 12
Progenitor 3 11
Progenitor 2 10
Interneuron 2 9
Radial Glia 3 8
Radial Glia 2 7
GABAergic Neuron 2 6
Radial Glia 1 5
Progenitor 1 4
Mesenchymal 3
Interneuron 1 2
Astrocyte 1 1
GABAergic Neuron 1 0
ADCY5 NR4A1 SLC6A1 GAD2 GAD1 GABRA2 GRIK2 GRIN2B GRIA4 GRIA1 SLC17A7 SLC17A6 NOS1 MAP2 SOX2 SOX4 MKI67 PAX6 TOX WLS LMX1A VIM TOP2A COL6A3 USPL1 PDGFRA TMEM132D GLI3 COLEC12 MRC2 GFAP LRRC3B CD44
Average Expression
2
1
0
Percent Expressed
0
25
50
75
100
B
% of GABAergic Neurons
100
80
60
40
20
0
Arber
Fjodorova
Wu
Nicoleau
Bagley
Rudibaugh1
Xiang-Tanaka
GABAergic Neuron 5
GABAergic Neuron 4
GABAergic Neuron 3
GABAergic Neuron 2
GABAergic Neuron 1
C
GAD1
GRIN2A
NPAS2
NR4A1
SOX11
GRM5
12345
GABAergic Neurons
GAD2
ARPP21
NPAS4
ADCY5
SOX4
LAMP5
12345
GABAergic Neurons
D
PPP1R1B
GABAergic Neuron
Astrocyte
Interneuron
Mesenchymal
Progenitor
Radial Glia
Glutamatergic Neuron
Oligodendrocyte
DRD1
GABAergic Neuron
Astrocyte
Interneuron
Mesenchymal
Progenitor
Radial Glia
Glutamatergic Neuron
Oligodendrocyte
DRD2
GABAergic Neuron
Astrocyte
Interneuron
Mesenchymal
Progenitor
Radial Glia
Glutamatergic Neuron
Oligodendrocyte

Related to Figure 2; Figure S2: Clustering analysis reveals subpopulations of cells exhibit different abundances depending on the protocol

(A) Dot plot of select marker genes for identifying the 8 different cell types. **(B)** Bar chart of the seven different models showing the relative abundance of the five different GABAergic neuron subtypes. **(C)** Clustered violin plots starting with the GABAergic neuron clusters on the far left showing expression of various genes of interest. **(D)** Violin plots depicting the expression levels of *DARPP32* (*PPP1R1B*), *DRD1*, and *DRD2* transcripts at 50,000 reads/cell show low expression in all cell types.

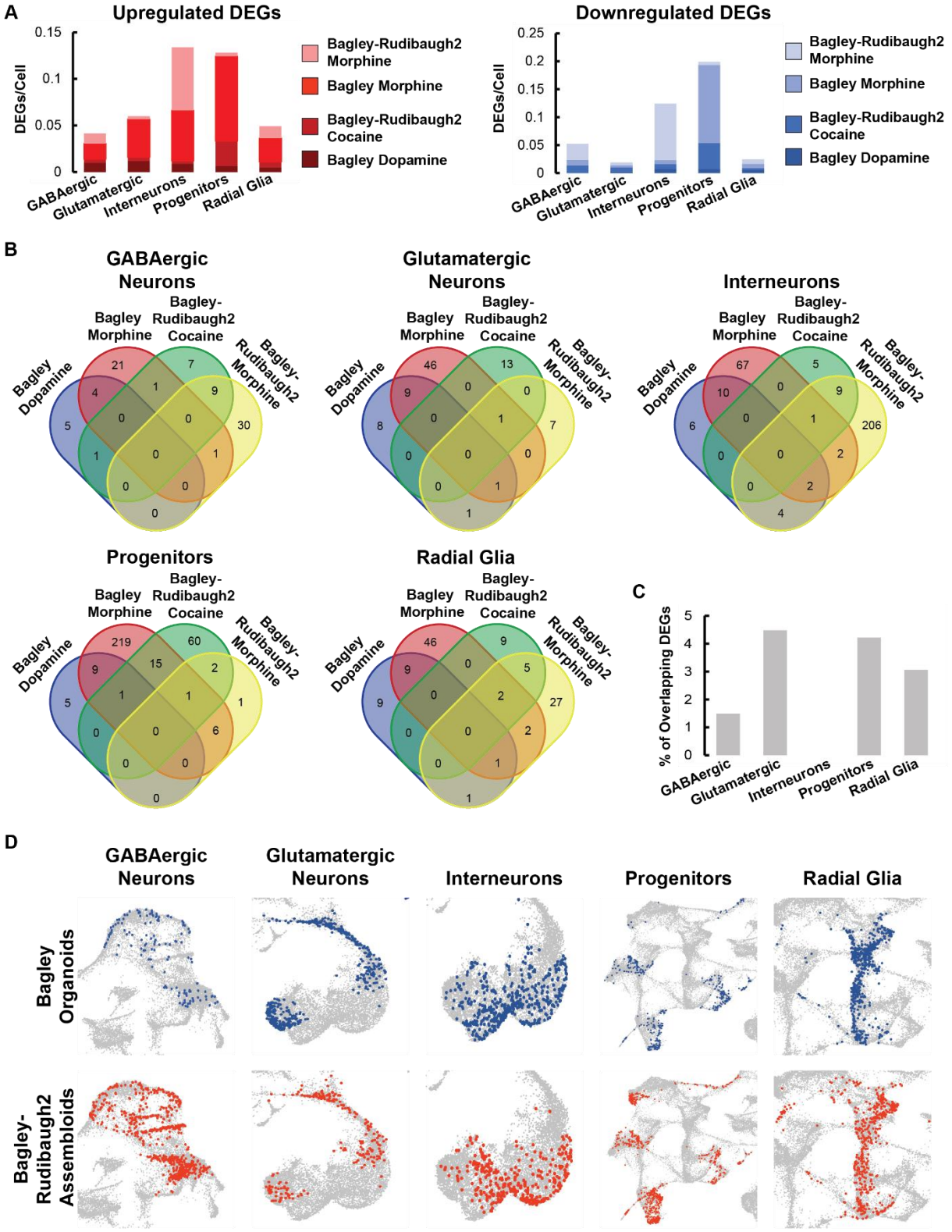
A
Upregulated DEGs
DEGs/Cell
0.15
0.1
0.05
0
GABAergic
Glutamatergic
Interneurons
Progenitors
Radial Glia
Bagley-Rudibaugh2 Morphine
Bagley Morphine
Bagley-Rudibaugh2 Cocaine
Bagley Dopamine
Downregulated DEGs
DEGs/Cell
0.25
0.2
0.15
0.1
0.05
0
GABAergic
Glutamatergic
Interneurons
Progenitors
Radial Glia
Bagley-Rudibaugh2 Morphine
Bagley Morphine
Bagley-Rudibaugh2 Cocaine
Bagley Dopamine
B
GABAergic Neurons
Glutamatergic Neurons
Interneurons
Progenitors
Radial Glia
Bagley Morphine
Bagley-Rudibaugh2 Cocaine
Bagley Dopamine
Bagley-Rudibaugh2 Morphine
C
% of Overlapping DEGs
5
4
3
2
1
0
GABAergic
Glutamatergic
Interneurons
Progenitors
Radial Glia
D
GABAergic Neurons
Glutamatergic Neurons
Interneurons
Progenitors
Radial Glia
Bagley Organoids
Bagley-Rudibaugh2 Assembloids

Related to Figure 3; Figure S3: ***Cell specific transcriptional analysis and comparisons following exposure to dopamine, cocaine, and morphine***

(A) The ratio of the total number of up and downregulated DEGs to the total number of cells in both control and dosed conditions. DEGs defined as log2FC >|0.5|, expression in over 20% of sequenced cells, and false discovery rate q<0.05 relative to ascorbic acid dosed controls. **(B)** Venn diagrams comparing the DEGs across the 4 different compound regimens keeping the cell type constant. **(C)** The ratio of overlapping DEGs between Bagley-morphine and Bagley-Rudibaugh2 morphine, when compared to the total number of DEGs while keeping the cell type constant. **(D)** UMAP plots showing the five different cell-types studied: GABAergic Neurons, Glutamatergic Neurons, Interneurons, Progenitors, and Radial Glia in Bagley Organoids and Bagley-Rudibaugh2 Assembloids

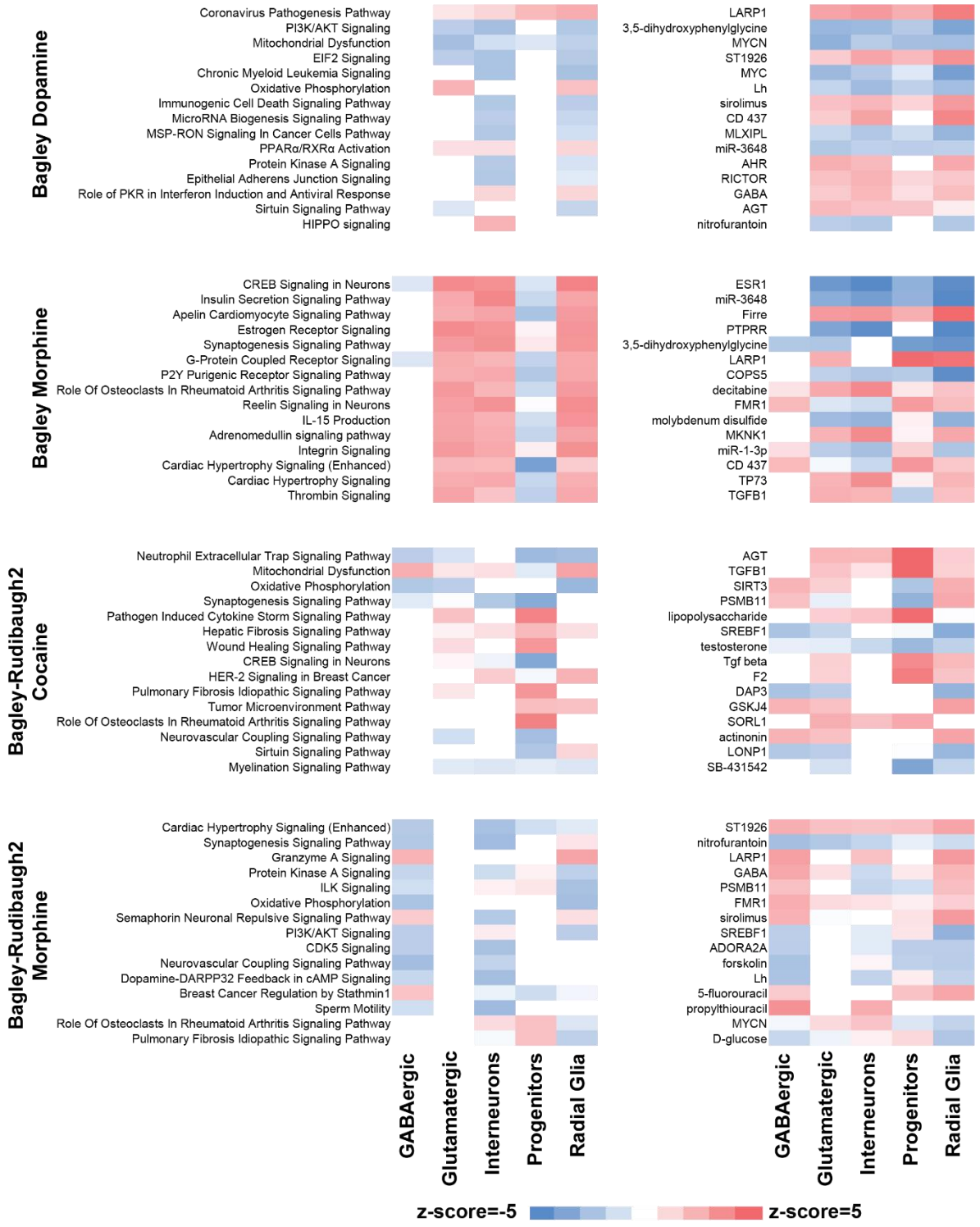
Bagley Dopamine
Coronavirus Pathogenesis Pathway
PI3K/AKT Signaling
Mitochondrial Dysfunction
EIF2 Signaling
Chronic Myeloid Leukemia Signaling
Oxidative Phosphorylation
Immunogenic Cell Death Signaling Pathway
MicroRNA Biogenesis Signaling Pathway
MSP-RON Signaling In Cancer Cells Pathway
PPARα/RXRα Activation
Protein Kinase A Signaling
Epithelial Adherens Junction Signaling
Role of PKR in Interferon Induction and Antiviral Response
Sirtuin Signaling Pathway
HIPPO signaling
LARP1
3,5-dihydroxyphenylglycine
MYCN
ST1926
MYC
Lh
sirolimus
CD 437
MLXIPL
miR-3648
AHR
RICTOR
GABA
AGT
nitrofurantoin
Bagley Morphine
CREB Signaling in Neurons
Insulin Secretion Signaling Pathway
Apelin Cardiomyocyte Signaling Pathway
Estrogen Receptor Signaling
Synaptogenesis Signaling Pathway
G-Protein Coupled Receptor Signaling
P2Y Purigenic Receptor Signaling Pathway
Role Of Osteoclasts In Rheumatoid Arthritis Signaling Pathway
Reelin Signaling in Neurons
IL-15 Production
Adrenomedullin signaling pathway
Integrin Signaling
Cardiac Hypertrophy Signaling (Enhanced)
Cardiac Hypertrophy Signaling
Thrombin Signaling
ESR1
miR-3648
Firre
PTPRR
3,5-dihydroxyphenylglycine
LARP1
COPS5
decitabine
FMR1
molybdenum disulfide
MKNK1
miR-1-3p
CD 437
TP73
TGFB1
Bagley-Rudibaugh2 Cocaine
Neutrophil Extracellular Trap Signaling Pathway
Mitochondrial Dysfunction
Oxidative Phosphorylation
Synaptogenesis Signaling Pathway
Pathogen Induced Cytokine Storm Signaling Pathway
Hepatic Fibrosis Signaling Pathway
Wound Healing Signaling Pathway
CREB Signaling in Neurons
HER-2 Signaling in Breast Cancer
Pulmonary Fibrosis Idiopathic Signaling Pathway
Tumor Microenvironment Pathway
Role Of Osteoclasts In Rheumatoid Arthritis Signaling Pathway
Neurovascular Coupling Signaling Pathway
Sirtuin Signaling Pathway
Myelination Signaling Pathway
AGT
TGFB1
SIRT3
PSMB11
lipopolysaccharide
SREBF1
testosterone
Tgf beta
F2
DAP3
GSKJ4
SORL1
actinonin
LONP1
SB-431542
Bagley-Rudibaugh2 Morphine
Cardiac Hypertrophy Signaling (Enhanced)
Synaptogenesis Signaling Pathway
Granzyme A Signaling
Protein Kinase A Signaling
ILK Signaling
Oxidative Phosphorylation
Semaphorin Neuronal Repulsive Signaling Pathway
PI3K/AKT Signaling
CDK5 Signaling
Neurovascular Coupling Signaling Pathway
Dopamine-DARPP32 Feedback in cAMP Signaling
Breast Cancer Regulation by Stathmin1
Sperm Motility
Role Of Osteoclasts In Rheumatoid Arthritis Signaling Pathway
Pulmonary Fibrosis Idiopathic Signaling Pathway
ST1926
nitrofurantoin
LARP1
GABA
PSMB11
FMR1
sirolimus
SREBF1
ADORA2A
forskolin
Lh
5-fluorouracil
propylthiouracil
MYCN
D-glucose
GABAergic
Glutamatergic
Interneurons
Progenitors
Radial Glia
z-score=-5
z-score=5

Related to Figure 4, Figure S4; Top regulated canonical pathways and upstream regulators based on GSEA

GSEA of the cell type specific DEGs reveals the top 15 regulated canonical pathways and upstream regulators based on z-score. For a pathway or regulator to be significant z-score>|2|.

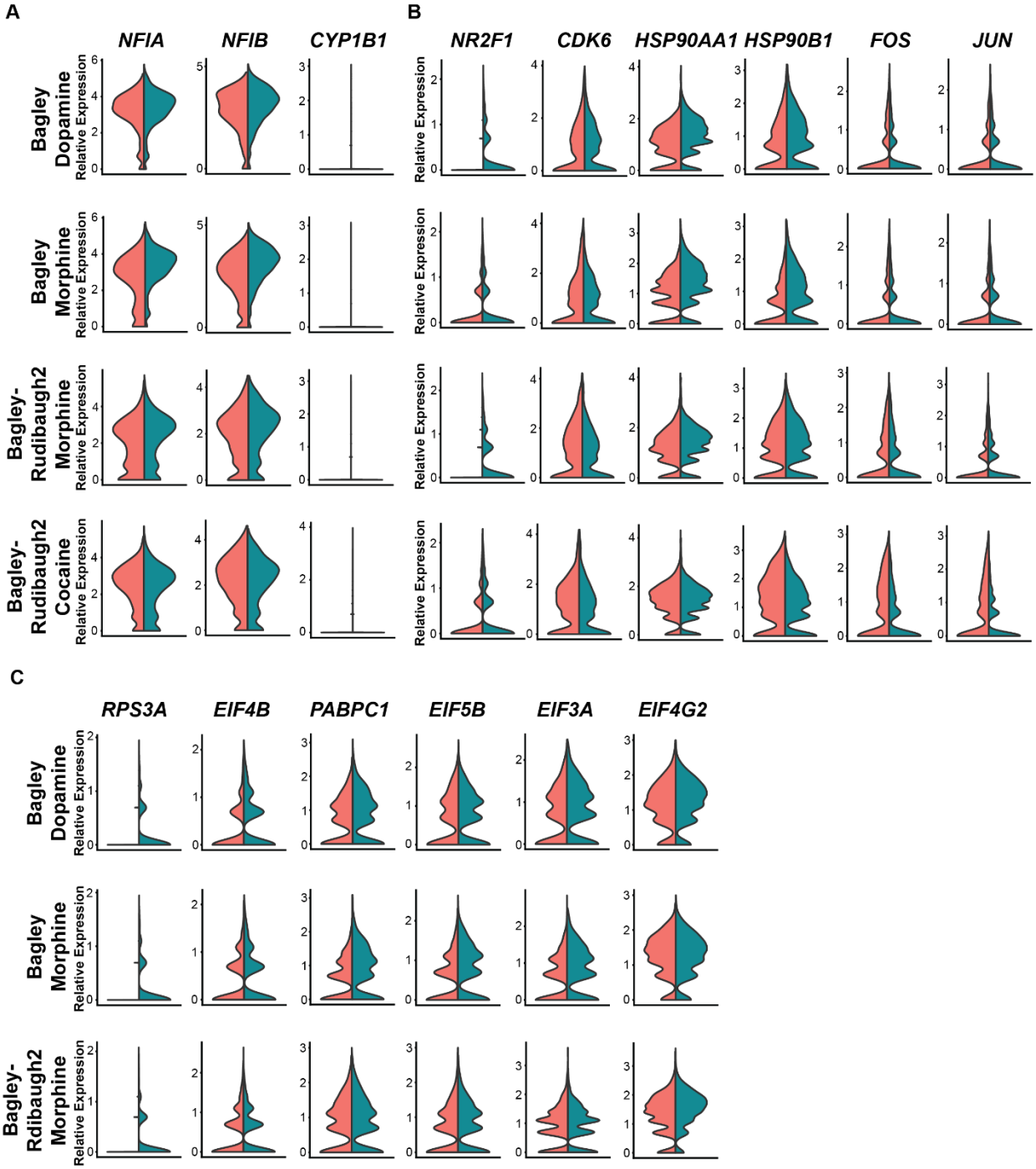
A
B
C
NFIA
NFIB
CYP1B1
NR2F1
CDK6
HSP90AA1
HSP90B1
FOS
JUN
RPS3A
EIF4B
PABPC1
EIF5B
EIF3A
EIF4G2
Bagley Dopamine
Bagley Morphine
Bagley-Rudibaugh2 Morphine
Bagley-Rudibaugh2 Cocaine
Bagley-Rdibaugh2 Morphine
Relative Expression

Related to Figure 5; Figure S5: ***Genes linked with neuroinflammation, eIF2α, and TGF-β are upregulated in compound dosed samples***

(A) Compound exposure causes differential expression of immune response genes in all four dosed conditions. **(B)** Compound exposure causes differential expression of stress response genes and heat shock proteins in all four compound regimens. **(C)** Downregulation of genes related to EIF2 signaling in Bagley Dopamine, Bagley Morphine, and Bagley-Rudibaugh2 morphine conditions. **(A-C)** All genes shown have false discovery rate $q<0.05$ relative to ascorbic acid dosed controls.

Table S1
Related to Figure 1 and Figure S1, Primary Antibodies

Antigen	Species	Company	Catalog	RRID	Dilution
DARPP32	Rabbit	Abcam	Ab40801	AB_731843	1:50
MAP2	Mouse	Sigma-Aldrich	M1406	AB_477171	1:250
TH	Rabbit	Millipore	AB152	AB_390204	1:300
TH	Mouse	Immunostar	22941	AB_572268	1:250
GSX2	Rabbit	Millipore	Abn162	AB_11203296	1:500
SOX2	Goat	R&D Systems	AF2018	AB_355110	1:100
CTIP2	Rat	Abcam	Ab18465	AB_2064130	1:250
FOXA2	Rabbit	Millipore	07-633	AB_390153	1:250
NURR1	Rabbit	Millipore	AB5778	AB_92023	1:200
GABA	Rabbit	Sigma-Aldrich	A2052	AB_477652	1:200

Table S2
Related to Figure 1 and Figure S1, Secondary Antibodies

Species	Flourophore	Company	Catalog	RRID	Dilution
Rabbit	488	Life Technologies	A21206	AB_2535792	1:250
Mouse	546	Thermofisher	A10036	AB_2534012	1:250
Rat	647	Jackson Immunoresearch	712605150	AB_2340693	1:125
Goat	647	Jackson Immunoresearch	705605003	AB_2340436	1:125

Table S3
Related to Figure 1 and Figure S1, qPCR Primers

Gene Symbol	Gene ID	Forward Primer	Reverse Primer
DARPP32	84152	TTGGAAAATCCAGAAAACCG	CTGGTAGAAGCCGGTGAGAG
A2A	135	AGGCAGCAAGAACCTTTCAA	CTAAGGAGCTCCACGTCTGG
PENK	5179	GCTGTCCAAACCAGAGCTTC	TCTGGCTCCATGGGATAAAG
TAC1	6863	TGGGGTTGAAAATTCAAAAAG	GGAGTTTCCTTCCTTTTCCG
TH	7054	TGTCTGAGGAGCCTGAGATTCG	GCTTGTCCTTGGCGTCACTG
DAT	6531	CAACAAGTTCACCAACTG	GGAGGAGAAGCTCGTCAG
NURR1	4929	CAGGCGTTTTCGAGGAAAT	GAGACGCGGAGAACTCCTAA
DDC	1644	GGGGACCACAACATGCTGCTCC	AATGCACTGCCTGCGTAGGCTG
GAPDH	2597	ATGACATCAAGAAGGTGGTG	CATACCAGGAAATGAGCTTG